Journal of Nuclear Medicine, published on September 3, 2019 as doi:10.2967/jnumed.119.233064

Hybrid Tracers Based on Cyanine Backbones Targeting Prostate-Specific Membrane Antigen – Tuning Pharmacokinetic Properties and Exploring Dye–Protein Interaction

Albertus W. Hensbergen,[1] Tessa Buckle,[1] Danny M. van Willigen,[1] Margret Schottelius,[2] Mick M. Welling,[1] Felicia A. van der Wijk,[1] Tobias Maurer,[3] Henk G. van der Poel,[4] Gabri van der Pluijm,[5] Wytske M. van Weerden,[6] Hans-Jürgen Wester,[2] Fijs W. B. van Leeuwen[1,*]

[1]Interventional Molecular Imaging Laboratory, Department of Radiology, Leiden University Medical Center, Leiden, The Netherlands

[2]Pharmazeutische Radiochemie, Technische Universität München, Garching, Germany

[3]Martini-Klinik, Universitätsklinikum Hamburg-Eppendorf, Hamburg, Germany

[4]Department of Urology, Netherlands Cancer Institute-Antoni van Leeuwenhoek Hospital, Amsterdam, The Netherlands

[5]Department of Urology, Leiden University Medical Centre, Leiden, The Netherlands

[6]Department of Urology, Erasmus MC Cancer Institute, Erasmus University Medical Center, Rotterdam, The Netherlands

[*]Corresponding author: Fijs W. B. van Leeuwen. Interventional Molecular Imaging Laboratory, Department of Radiology, Leiden University Medical Center, Albinusdreef 2, 2333 ZA Leiden, The Netherlands. Phone: +31715266029. E-mail: f.w.b.van_leeuwen@lumc.nl

First author: Albertus W. Hensbergen, PhD student at the Interventional Molecular Imaging Laboratory, Department of Radiology, Leiden University Medical Center, Albinusdreef 2, 2333 ZA Leiden, The Netherlands. Phone: +31715262042. E-mail: a.w.hensbergen@lumc.nl

Running title: cyanine-spacer-based PSMA hybrid tracers

Word count: 4960

ABSTRACT

Currently, the use of prostate-specific membrane antigen (PSMA)-targeted radiotracers, *e.g.*, ^{99m}Tc-labelled PSMA tracer analogues for radioguided surgery, is revolutionising prostate cancer surgery. The purpose of this study was to develop a second-generation ^{99m}Tc-labelled PSMA tracer incorporating a fluorescent dye. **Methods:** PSMA-targeting hybrid tracers were synthesised: EuK-Cy5-mas$_3$, EuK-(SO$_3$)Cy5-mas$_3$, EuK-Cy5(SO$_3$)-mas$_3$, EuK-(Ar)Cy5-mas$_3$, EuK-Cy5(Ar)-mas$_3$; the Cy5 dye acts as a functional backbone between the EuK targeting vector and the mas$_3$ chelate to study the dye's interaction with PSMA's amphipathic entrance funnel. Compounds were evaluated for their photophysical and chemical properties and PSMA affinity. Following radiolabelling with ^{99m}Tc, *in vivo* SPECT imaging, biodistribution and fluorescence imaging was conducted in BALB/c nude mice with orthotopically transplanted PC346C tumours. **Results:** The dye composition influenced the photophysical properties (0.3–1.5 · 10^4 M^{-1} · cm^{-1}), plasma protein interactions (85.0 ± 2.3–90.7 ± 1.3% bound to serum, 76 ± 0–89 ± 6% stability in serum), PSMA affinity (IC_{50} range 19.2 ± 5.8–175.3 ± 61.1 nM) and *in vivo* characteristics (tumour-to-prostate and tumour-to-muscle ratio: respectively 0.02 ± 0.00–154.73 ± 28.48 and 0.46 ± 0.28–5157.50 ± 949.17; renal, splenic and salivary retention). Even though all tracer analogues allowed tumour identification with SPECT and fluorescence imaging, ^{99m}Tc-EuK-(SO$_3$)Cy5-mas$_3$ portrayed the most promising properties (*e.g*, IC_{50} = 19.2 ± 5.8, tumour-to-muscle ratio 5157.50 ± 949.17) of all compounds tested. **Conclusions:** Our findings demonstrate the intrinsic integration of a fluorophore in the pharmacophore in PSMA-targeting small-molecule tracers. In this design having one sulfonate on the indole moiety adjacent to EuK (^{99m}Tc-EuK-(SO$_3$)Cy5-mas$_3$) yielded the most promising tracer candidate for the imaging of PSMA.

Keywords: prostate cancer, prostate-specific membrane antigen, hybrid tracers, image-guided surgery, cyanine

INTRODUCTION

With an estimated 1.3 million new cases (14% of total number of new cases) and over 350,000 estimated deaths worldwide in 2018, prostate cancer is the second most frequent cancer and fifth leading cause of cancer death in men (*1*). To eradicate the primary cancer, radical prostatectomy—encompassing radical local resection as well as dissection of lymphatic spread—is a commonly used surgical approach (*2,3*). Although effective, this approach needs refinement and improvements as recurrence rates after radical prostatectomy are still high (20–40%) (*4*). In this scenario, prostate-tumour-specific tracers containing both a radioactive and optical marker are highly warranted. The prostate-specific membrane antigen (PSMA), a transmembrane protein highly overexpressed on nearly all prostate cancer tumours (*5*), has received increased interest as a target for molecular imaging applications and more recently, in image-guided surgery interventions (*6,7*).

Clinical PSMA imaging reports generally make use of radiolabelled high affinity glutamate–urea-based targeting moieties, such as the inhibitor motif glutamic acid-urea-lysine (EuK) (*8,9*), which are applied in a micro-dose regime ($\leq$ 100 μg/patient). The molecular binding interactions of glutamate–urea moieties to the PSMA protein have been studied extensively (*10*). The glutamate–ureido derivatives coordinate specifically with the binuclear zinc present deep within the PSMA protein. An amphipathic entrance funnel, *i.e.*, the funnel comprised of the arene-binding site, arginine patch and S1 accessory hydrophobic pocket, leads to this binding site (*11*). The S1 accessory hydrophobic pocket can be exploited as secondary binding site (*12*). In line with this finding, it has been found that refinement of the backbone composition and length used to connect the imaging (or therapeutic) radiolabel to the glutamate–urea targeting vector impacts the PSMA binding in radiotracer development, exploiting charged, uncharged or lipophilic spacers (*13-15*). Next to the development of PSMA-targeting agents for PET diagnostics, *e.g.*, ^{68}Ga-PSMA-HBED-CC (*7*), or therapy, *e.g.*, ^{177}Lu-PSMA I&T (*16*), or ^{177}Lu-PSMA-617 (*17*), the SPECT agents ^{111}In-Tc-PSMA I&T and ^{99m}Tc-PSMA I&S have successfully been used for the radioguided resection of

metastatic lymph nodes in a salvage setting (*7,18,19*). For the latter, ^{99m}Tc has proven to be the preferable radionuclide for this application due to its low costs, availability and short half-life (*20*).

The field of intraoperative fluorescence-guided surgery has been growing vigorously over the last two decades and is being used within the clinic more often due to its potential to realise radical resections while preserving healthy tissue (*2,21*). Based on this reasoning, numerous fluorescence-based probes for the imaging of prostate cancer have been studied preclinically (*22-24*). While the influence of various families of (commercially available) dyes on the PSMA-targeting ability has been studied (*25*), systematic refinement of the dye structure intending to tailor PSMA interaction has not been reported to date. The exception being Matsuoka *et al.* reporting that sulfonation of cyanine dyes had a positive influence on the PSMA affinity (*26*). In the development of fluorescent PSMA-targeting tracers, however, secondary binding to the amphipathic entrance funnel has also not received much interest.

Relying on fluorescence imaging alone during surgical guidance has its drawbacks: a limited penetration depth (< 10 mm), the inability to roughly assess lesions and/or metastases preoperatively, tissue autofluorescence and a high dose-dependent detection accuracy (*27*). At the same time, the audible and numerical radioguidance provided by a gamma probe would benefit from being augmented with intraoperative optical identification of lesions. To overcome these shortcomings, a fluorescent and a radioactive label can be combined in one molecule; creating so-called dual-labelled, bimodal, or rather hybrid tracers which have been explored clinically (*28*). This hybrid concept has also been adapted in preclinical PSMA imaging, *e.g.*, ^{111}In-LICOR-800CW-Lys-DOTA-EuK (*29*), PSMA-11 derivatives (*13*), a ^{18}F-containing, Cy3-based probe (*30*), and PSMA Imaging & Fluorescence (PSMA I&F) (*31*). Despite the ability of these tracer designs to offer a “best of both worlds” scenario in image-guided surgery, *in vivo* analysis of the reported hybrid tracer analogues revealed that the reported synthetic designs are cleared and accumulated, at least fractionally, by the kidneys (*13,29,31*). A drawback from the intraoperative use of

these tracers is that their renal retention profile might lead to contamination of the surgical field with fluorescent urine and as such prohibit assessment of surgical margins.

To advance the concept of PSMA-targeting image-guided surgery, we aimed to design EuK-based, ^{99m}Tc-containing hybrid PSMA-targeting tracers with different substituents (sulfonate or benzene) that offer a high selective tumour affinity, a high optical brightness and tissue penetration, favourable biodistribution and *in vivo* stability as well as minimal (or fast) renal clearance. By adhering to the concept that the backbone can promote the pharmacophore interaction with the amphipathic entrance funnel of PSMA (*13-15,32*), the influence of modifications on a cyanine backbone were studied (Figure 1).

MATERIALS AND METHODS

The reader is referred to the Supporting Information for the complete and detailed synthetic procedures and chemical analyses (MALDI-TOF, NMR of dyes (Supplemental Figure 1–4), HPLC of hybrid tracers (Supplemental Figure 5–9)), photophysical properties, radiochemistry, lipophilicity, plasma protein binding, plasma protein stability, PSMA affinity, protein–ligand docking, *in vivo* tumour model, in vivo SPECT imaging and quantitative assessment of the biodistribution, ex vivo fluorescence imaging, and statistical analysis.

RESULTS

Chemistry and Photophysical Properties

The reader is referred to the Supporting Information available online for results on the chemistry and photophysical properties of the hybrid tracers.

Lipophilicity and Plasma Protein Interaction

The partition coefficient in octanol/water ($logP_{(o/w)}$) indicated that the site of functionalisation slightly affected the lipophilicity (Table 1). As a first indication for *in vivo* behaviour, the degree of plasma protein binding (PPB) was studied, yielding the following trend: EuK-Cy5-mas_3 < EuK-(SO_3)Cy5-mas_3 ≈ EuK-Cy5(SO_3)-mas_3 < EuK-Cy5(Ar)-mas_3 < EuK-(Ar)Cy5-mas_3 (Table 1). It is interesting to note that the site of the substitution with a benzene moiety seemed to influence PPB to a statistically significant degree (81.7 ± 1.4% bound for EuK-Cy5(Ar)-mas_3 *vs.* 88.6 ± 2.5% bound EuK-(Ar)Cy5-mas_3 p = 0.0031), a change that could translate to differences in an *in vivo* setting (*33*). A correlation (R = 0.9232, p = 0.0252; Supplemental Figure 11) between the lipophilicity and PPB is observed: an increase in lipophilicity leads to a higher PPB which is in line with the literature (*31*).

Besides PPB, the chemical stability in plasma proteins is also a critical feature in tracer performance (*34,35*). After incubation in serum at 37 °C for 24 h, the absorbance intensity decreased (range 75 ± 0–97 ± 2%; p > 0.05; Table 1). The decrease of the fluorescence signal was in line with the decrease in absorbance (range 76 ± 0–89 ± 6%; Table 1). The ^{99m}Tc–mas_3 complex was stable in all tracers (Supplemental Table 2) as previously established (9). These findings thus indicated that the tracers are sufficiently stable.

Fluorescence Confocal Microscopy and Receptor Affinity

In vitro imaging revealed an influence of the dye composition on the cellular binding; EuK-(SO_3)Cy5-mas_3 portrayed the highest binding on PSMA-overexpressing LNCaP cells, while the symmetrical EuK-Cy5-mas_3 showed the least amount of binding (Figure 2A–B). Blocking with (((S)-1-carboxy-5-(4-(iodo-benzamido)pentyl)carbamoyl)-l-glutamic acid (EuK–I-BA; 10 μM) resulted in a significant reduction in tracer uptake (Figure 2F). Blocking was most efficient for EuK-(SO_3)Cy5-mas_3 and EuK-Cy5(SO_3)-mas_3 (up to 90%), indicating that these tracers had the lowest amount of non-specific binding.

Assessment of the binding affinity (IC_{50}) Figure 2A–E) revealed a unique influence of the cyanine backbone composition on the affinity for PSMA. EuK-(SO_3)Cy5-mas_3 had a high affinity for PSMA (19.2 ± 5.8 nM) which was in the same range of clinically used tracers such as ^{nat}Re-PSMA I&S (15.5 ± 2.8 nM) (*20*). All other analogues had a lower affinity (Figure 2A–E); it thus seems that not only the introduction of a sulfonate moiety, but also its location, had an effect on the affinity. This increase could be the result of favourable interactions of the ligand with the protein. Protein–ligand docking indeed indicated possible interactions between the cyanine backbone and the amphipathic funnel, indicating that the fluorophore can become an integral part of the pharmacophore (Supplemental Figure 12). In correspondence with the affinity results, docking calculations for the other four hybrid tracers did not yield this favoured configuration, underlining the importance of functional chemical moieties and their placement.

In Vivo Imaging and Biodistribution

In vivo SPECT imaging at 2 h after administration of 1 nmol tracer revealed clear differences in tracer uptake and distribution (Figure 3). Tumours were visible for all tracers and tracer retention in the kidneys was measured in for all compounds. The more lipophilic tracers ^{99m}Tc-EuK-(Ar)Cy5-mas_3 and ^{99m}Tc-EuK-Cy5(Ar)-mas_3 showed higher retention in the liver and bowels compared to the other tracers. Quantitative assessment of the biodistribution *ex vivo* after counting radioactivity and weighing of the excised tissues revealed biodistribution patterns comparable to the SPECT images (Supplemental Table 3).

Uptake in the kidneys after 2 h was in the range of 8.98 ± 5.78–18.35 ± 8.51 %ID/g (Supplemental Table 3). Other notorious locations for PSMA tracer accumulation, the salivary glands and spleen (which are essentially PSMA-negative in mice) (*31*), portrayed low uptake as well (0.02 ± 0.01–0.23 ± 0.12 %ID/g for salivary glands and 0.18 ± 0.19–1.03 ± 0.72 %ID/g for spleen; $p > 0.05$ for all comparisons). Chemical alterations on the cyanine backbone did not induce statistically significant organ uptake changes ($p >$

0.05). As expected, hybrid tracer uptake in the brain was almost undetectable, indicating that the tracers were not able to cross the blood–brain barrier.

Quantitative assessment of the biodistribution further revealed the highest accumulation in tumorous tissue for ^{99m}Tc-EuK-(SO_3)Cy5-mas_3 (15.27 ± 2.85 %ID/g; Supplemental Table 3). The other tracers had lower tumour uptake and were in the same range ($p > 0.05$). Blood uptake values seemed to be somewhat in line with lipophilicity; the more lipophilic a tracer is, the higher its blood retention value (Table 1, Supplemental Table 3). ^{99m}Tc-EuK-(SO_3)Cy5-mas_3 and ^{99m}Tc-EuK-Cy5(SO_3)-mas_3, the most hydrophilic tracers, thus provided the lowest blood retention at 2 h (Supplemental Table 3). Another important quantification for assessing tracer performance is the tumour-to-organ ratio for different tissues, as a tumour is well-vascularised and surrounded by muscle and prostate tissue. Therefore, the tumour uptake was related to the background uptake in blood, muscle, prostate and fat (Supplemental Table 3). Overall, ^{99m}Tc-EuK-(SO_3)Cy5-mas_3 provided the best uptake ratios, which is in relation to the faster clearance of this tracer in these tissues.

Fluorescence imaging of the tumour-containing prostate tissue with a clinical laparoscope setup for Cy5 imaging allowed for a visual tumour identification (Figure 4). In line with the brightness (Table 1), affinity (Figure 2A–E) and biodistribution (Supplemental Table 3), the intensity of the fluorescence signal stresses that the introduction of an extra benzene moiety on the chelate-bearing indole slightly reduces the detectability of the lesion.

DISCUSSION

Results obtained with PSMA-targeting hybrid tracers showed that by exploring the molecular design of cyanine-based PSMA-targeting hybrid tracers, changes in (photo)physical properties, plasma protein interactions and PSMA affinity could be related to *in vivo* tracer performance. Interestingly, the current findings indicate that a dye can also become an integral part of the pharmacophore. Out of the evaluated

panel of compounds, ^{99m}Tc-EuK-(SO_3)Cy5-mas_3 has been found to be the most favourable hybrid PSMA-targeting tracer.

In contrast to the introduction of a benzene moiety, the introduction of a sulfonate moiety induced a positive effect on the photophysical properties; the brightness increased by at least 27% compared to the non-substituted analogue EuK-Cy5-mas_3 (Table 1). These findings are in line with previous reports on the photophysical properties of Cy5- and Cy7 analogues (*34,35*). Hereby it should be noted that Cy5 analogues in general yield an approximate two-fold higher brightness than comparative Cy7 analogues, which favours use of the prior in optical *in vivo* imaging (*36,37*).

Our findings are in line with previous reports on radiotracer designs indicating that the location of chemical substituents in the backbone was of the utmost importance for interactions with PSMA's amphipathic funnel (Figure 2) (*12,13,32*). Interestingly, the introduction of benzene moieties did not increase the affinity while the introduction of an anionic sulfonate moiety on the C-terminus of the cyanine backbone increased the PSMA affinity compared to EuK-Cy5-mas_3. Furthermore, the affinity of EuK-(SO_3)Cy5-mas_3 was more than 9-fold higher than that of EuK-Cy5(SO_3)-mas_3, suggesting interactions with the amphipathic entrance funnel; the cyanine backbone allows hydrophobic interactions to be complemented with hydrogen bonding enabled by careful placement of the sulfonate moiety (Figure 2, Supplemental Figure 12). The Cy5 dyes have a (calculated) lipophilicity ranging between clogP = 1.4–6.3 which overlaps with the lipophilicity reported for favourable backbones that contain a naphthylic moiety (clogD = 2.9) (*32*). In previous studies, ^{nat}Re-labelled analogues were chosen to determine a compound's affinity as coordination of a metal ion to the chelate was shown to increase the PSMA affinity (*20*). A limitation of the current study is that these experiments with ^{nat}Re were not performed; meaning the affinity of the compounds may in fact be higher than reported here. However, the trend between the compound's affinities is expected to be similar. The current setting also allowed us to compare with literature values. Future studies of the k_{on} and k_{off} might provide more insight in the receptor affinity in

relation to the tracer composition. Also, when applying 1 nmol to a mouse, only a relatively small portion of the tracer will be radiolabelled with ^{99m}Tc, meaning fluorescence guidance is not essentially dependent on the radiolabeled fraction of the tracer. The use of higher doses than, *e.g.*, 60 pmol–0.2 nmol (*38*), is substantiated by the fact that studies with fluorescent-only PSMA-targeting tracers containing cyanine dyes regularly use 1–10 nmol (*22,39*).

Cyanine dyes, such as indocyanine green (a cyanine dye with two sulfonates and two benzene moieties), are well known for their albumin-binding properties (*40*). In line with this finding, the PPB increased when a sulfonate or extra benzene moiety was added onto the cyanine backbone (Table 1); molecular features that have been assigned to Sudlow's site I or II (*41*). The stability measurements in serum have shown high stability for both imaging labels, which complements literature showing that the EuK moiety is stable (*9*). The trends observed in lipophilicity and PPB were, however, only in part related to the biodistribution profile (Table 1, Supplemental Table 3). This observation stressed the important role that other molecular characteristics, *e.g.*, steric hindrance, polar surface area or pKa, play on tracer performance. The most lipophilic hybrid tracers (with an extra benzene moiety on either indole) provided an increased hepatobiliary clearance—which could potentially be a favourable feature—including increased intestinal uptake compared to the sulfonate-containing hybrid tracers, which is in line with the literature (*42*). Furthermore, the most lipophilic tracers presented an increased retention in muscle, blood, prostate and fat at 2 h p.i., which reduced tumour-to-muscle and tumour-to-blood ratios (Supplemental Table 3). The biodistribution data at the 2 h time point used during this study unfortunately complicates a direct comparison with studies that used a 1 h time point (such as for PSMA I&F (*31*), or ^{18}F-4 (*30*)) as biological half-life can influence renal clearance. Given the delay between imaging and surgery, we did, however, find it necessary to take the 2 h time point to assess the tracer potential in an image-guided surgery setting.

Next to the molecular design and the ability to relate the tracer performance to a specific cyanine backbone structure, one of the clear differences between our study and other studies regarding PSMA-targeting small-molecule hybrid tracers is reduced splenic and renal uptake (*29-31,43*). Considering that the renal uptake of DOTA (or DOTA analogue)-containing PSMA-targeting hybrid tracers at early time-points is around 100 %ID/g or even higher (*29,43*), while our study and the study of Kommidi *et al*. (*30*) yielded a renal uptake below 19 %ID/g, it seems that the introduction of radiolabels without relying on charged chelates in the design of hybrid PSMA-targeting tracers minimises renal uptake. As literature underlines that the chelate composition can also have a profound effect on the biodistribution pattern (*29*), the insights now obtained could support further design of PSMA-targeting hybrid tracers.

In agreement with previous reports (*36,42,44*), the recent biodistribution data underlines once more that the composition of the cyanine backbone is of sheer importance in designing hybrid tracers and that asymmetrical dye substitution holds promise during tracer refinement.

CONCLUSION

We have demonstrated that cyanine dyes can be used as a chemical backbone to connect an EuK targeting vector with a chelate for radiolabelling. By doing so it has been discovered that the dye composition influences the tracer affinity by interacting with the amphipathic funnel of the PSMA protein. In particular the introduction of a sulfonate moiety on the EuK-bearing indole allowed us to tune the affinity and *in vivo* performance. Overall, these efforts yielded a new PSMA-targeting hybrid tracer that could help accommodate the need for optical augmentation during PSMA-targeting radioguided surgery.

DISCLOSURE

This research is funded by an NWO-TTW-VICI grant (TTW 16141). FvL is a consultant for Hamamatsu Photonics and Chief Innovation Officer at ORSI Academy, HJW is founder and shareholder of Scintomics GmbH. No other potential conflicts of interest relevant to this article exist.

ACKNOWLEDGEMENTS

This research is funded by an NWO-TTW-VICI grant (TTW 16141). Molecular graphics and analyses performed with UCSF Chimera, developed by the Resource for Biocomputing, Visualization, and Informatics at the University of California, San Francisco, with support from NIH P41-GM103311.

KEY POINTS

Question: Is it possible to make the fluorescent dye an integral part of the pharmacophore and as such reduce the renal retention?

Pertinent findings: This preclinical study portrays the use of cyanine dyes as an integral part of the pharmacophore in the design of hybrid tracers. Moreover, the renal retention of such hybrid tracers has been reduced.

Implications for patient care: Firstly, new hybrid tracer designs is required in order to advance the field of image-guided surgery. Furthermore, by reducing the renal retention of hybrid tracers, urine spillage during radical prostatectomy might reduce hindrance navigation in the surgical field caused by fluorescent urine.

REFERENCES

1. Bray F, Ferlay J, Soerjomataram I, Siegel RL, Torre LA, Jemal A. Global cancer statistics 2018: GLOBOCAN estimates of incidence and mortality worldwide for 36 cancers in 185 countries. *CA Cancer J Clin.* 2018;68:394-424.

2. van Leeuwen FWB, Winter A, van Der Poel HG, et al. Technologies for image-guided surgery for managing lymphatic metastases in prostate cancer. *Nat Rev Urol.* 2019;16:159-171.

3. van Leeuwen FWB, van Oosterom MN, Meershoek P, et al. Minimal-invasive robot-assisted image-guided resection of prostate-specific membrane antigen–positive lymph nodes in recurrent prostate cancer. *Clin Nucl Med.* 2019;44:580-581.

4. Freedland SJ, Humphreys EB, Mangold LA, et al. Risk of prostate cancer-specific mortality following biochemical recurrence after radical prostatectomy. *JAMA.* 2005;294:433-439.

5. Bostwick DG, Pacelli A, Blute M, Roche P, Murphy GP. Prostate specific membrane antigen expression in prostatic intraepithelial neoplasia and adenocarcinoma: a study of 184 cases. *Cancer.* 1998;82:2256-2261.

6. Lindenberg ML, Turkbey B, Mena E, Choyke PL. Imaging locally advanced, recurrent, and metastatic prostate cancer: a review. *JAMA Oncol.* 2017;3:1415-1422.

7. Maurer T, Eiber M, Schwaiger M, Gschwend JE. Current use of PSMA-PET in prostate cancer management. *Nat Rev Urol.* 2016;13:226-235.

8. Weineisen M, Schottelius M, Simecek J, Eiber M, Schwaiger M, Wester H. Development and first in human evaluation of PSMA I&T - A ligand for diagnostic imaging and endoradiotherapy of prostate cancer. *J Nucl Med.* 2014;55:1083.

9. Weineisen M, Simecek J, Schottelius M, Schwaiger M, Wester HJ. Synthesis and preclinical evaluation of DOTAGA-conjugated PSMA ligands for functional imaging and endoradiotherapy of prostate cancer. *EJNMMI Res.* 2014;4:63.

10. Ferraris DV, Shukla K, Tsukamoto T. Structure-activity relationships of glutamate carboxypeptidase II (GCPII) inhibitors. *Curr Med Chem.* 2012;19:1282-1294.

11. Mesters JR, Barinka C, Li W, et al. Structure of glutamate carboxypeptidase II, a drug target in neuronal damage and prostate cancer. *EMBO J.* 2006;25:1375-1384.

12. Maung J, Mallari JP, Girtsman TA, et al. Probing for a hydrophobic a binding register in prostate-specific membrane antigen with phenylalkylphosphonamidates. *Bioorg Med Chem.* 2004;12:4969-4979.

13. Baranski AC, Schafer M, Bauder-Wust U, et al. Improving the imaging contrast of (68)Ga-PSMA-11 by targeted linker design: charged spacer moieties enhance the pharmacokinetic properties. *Bioconjug Chem.* 2017;28:2485-2492.

14. Kuo HT, Pan J, Zhang Z, et al. Effects of linker modification on tumor-to-kidney contrast of (68)Ga-labeled PSMA-targeted imaging probes. *Mol Pharm.* 2018;15:3502-3511.

15. Liu T, Nedrow-Byers JR, Hopkins MR, Berkman CE. Spacer length effects on in vitro imaging and surface accessibility of fluorescent inhibitors of prostate specific membrane antigen. *Bioorg Med Chem Lett.* 2011;21:7013-7016.

16. Heck MM, Tauber R, Schwaiger S, et al. Treatment outcome, toxicity, and predictive factors for radioligand therapy with (177)Lu-PSMA-I&T in metastatic castration-resistant prostate cancer. *Eur Urol.* 2019;75:920-926.

17. Kratochwil C, Giesel FL, Stefanova M, et al. PSMA-targeted radionuclide therapy of metastatic castration-resistant prostate cancer with 177Lu-labeled PSMA-617. *J Nucl Med.* 2016;57:1170-1176.

18. Horn T, Kronke M, Rauscher I, et al. Single lesion on prostate-specific membrane antigen-ligand positron emission tomography and low prostate-specific antigen are Prognostic factors for a favorable biochemical response to prostate-specific membrane antigen-targeted radioguided surgery in recurrent prostate cancer. *Eur Urol.* 2019;In press.

19. van Leeuwen FWB, van Oosterom MN, Meershoek P, et al. Minimal-invasive robot-assisted image-guided resection of prostate-specific membrane antigen-positive lymph nodes in recurrent prostate cancer. *Clin Nucl Med.* 2019;Publish Ahead of Print.

20. Robu S, Schottelius M, Eiber M, et al. Preclinical evaluation and first patient application of Tc-99m-PSMA-I&S for SPECT imaging and radioguided surgery in prostate cancer. *J Nucl Med.* 2017;58:235-242.

21. Rosenthal EL, Warram JM, de Boer E, et al. Successful translation of fluorescence navigation during oncologic surgery: a consensus report. *J Nucl Med.* 2016;57:144-150.

22. Chen Y, Dhara S, Banerjee SR, et al. A low molecular weight PSMA-based fluorescent imaging agent for cancer. *Biochem Biophys Res Commun.* 2009;390:624-629.

23. Kularatne SA, Thomas M, Myers CH, et al. Evaluation of novel prostate-specific membrane antigen-targeted near-infrared imaging agent for fluorescence-guided surgery of prostate cancer. *Clin Cancer Res.* 2019;25:177-187.

24. Liu T, Wu LY, Hopkins MR, Choi JK, Berkman CE. A targeted low molecular weight near-infrared fluorescent probe for prostate cancer. *Bioorg Med Chem Lett.* 2010;20:7124-7126.

25. Chen Y, Pullambhatla M, Banerjee SR, et al. Synthesis and biological evaluation of low molecular weight fluorescent imaging agents for the prostate-specific membrane antigen. *Bioconjug Chem.* 2012;23:2377-2385.

26. Matsuoka D, Watanabe H, Shimizu Y, et al. Structure-activity relationships of succinimidyl-Cys-C(O)-Glu derivatives with different near-infrared fluorophores as optical imaging probes for prostate-specific membrane antigen. *Bioorg Med Chem.* 2018;26:2291-2301.

27. KleinJan GH, Bunschoten A, van den Berg NS, et al. Fluorescence guided surgery and tracer-dose, fact or fiction? *Eur J Nucl Med Mol Imaging.* 2016;43:1857-1867.

28. van Leeuwen FW, Valdes-Olmos R, Buckle T, Vidal-Sicart S. Hybrid surgical guidance based on the integration of radionuclear and optical technologies. *Br J Radiol.* 2016;89:20150797.

29. Banerjee SR, Pullambhatla M, Byun Y, et al. Sequential SPECT and optical imaging of experimental models of prostate cancer with a dual modality inhibitor of the prostate-specific membrane antigen. *Angew Chem Int Ed Engl.* 2011;50:9167-9170.

30. Kommidi H, Guo H, Nurili F, et al. (18)F-Positron emitting/trimethine cyanine-fluorescent contrast for image-guided prostate cancer management. *J Med Chem.* 2018;61:4256-4262.

31. Schottelius M, Wurzer A, Wissmiller K, et al. Synthesis and preclinical characterization of the PSMA-targeted hybrid tracer PSMA-I&F for nuclear and fluorescence imaging of prostate cancer. *J Nucl Med.* 2019;60:71-78.

32. Benesova M, Bauder-Wust U, Schafer M, et al. Linker modification strategies to control the prostate-specific membrane antigen (PSMA)-targeting and pharmacokinetic properties of DOTA-conjugated PSMA inhibitors. *J Med Chem.* 2016;59:1761-1775.

33. Wirtz M, Schmidt A, Schottelius M, et al. Synthesis and in vitro and in vivo evaluation of urea-based PSMA inhibitors with increased lipophilicity. *Ejnmmi Research.* 2018;8.

34. Spa SJ, Hensbergen AW, van der Wal S, Kuil J, van Leeuwen FWB. The influence of systematic structure alterations on the photophysical properties and conjugation characteristics of asymmetric cyanine 5 dyes. *Dyes and Pigments.* 2018;152:19-28.

35. van der Wal S, Kuil J, Valentijn ARPM, van Leeuwen FWB. Synthesis and systematic evaluation of symmetric sulfonated centrally C C bonded cyanine near-infrared dyes for protein labelling. *Dyes and Pigments.* 2016;132:7-19.

36. Buckle T, van Willigen DM, Spa SJ, et al. Tracers for fluorescence-guided surgery: how elongation of the polymethine chain in cyanine dyes alters the pharmacokinetics of a dual-modality c[RGDyK] tracer. *J Nucl Med.* 2018;59:986-992.

37. van Willigen DM, van den Berg NS, Buckle T, et al. Multispectral fluorescence guided surgery; a feasibility study in a phantom using a clinical-grade laparoscopic camera system. *Am J Nucl Med Mol Imaging.* 2017;7:138-147.

38. Kung MP, Kung HF. Mass effect of injected dose in small rodent imaging by SPECT and PET. *Nucl Med Biol.* 2005;32:673-678.

39. Kwon YD, Chung HJ, Lee SJ, Lee SH, Jeong BH, Kim HK. Synthesis of novel multivalent fluorescent inhibitors with high affinity to prostate cancer and their biological evaluation. *Bioorg Med Chem Lett.* 2018;28:572-576.

40. Bunschoten A, Buckle T, Kuil J, et al. Targeted non-covalent self-assembled nanoparticles based on human serum albumin. *Biomaterials.* 2012;33:867-875.

41. Buckle T, Chin PT, van Leeuwen FW. (Non-targeted) radioactive/fluorescent nanoparticles and their potential in combined pre- and intraoperative imaging during sentinel lymph node resection. *Nanotechnology.* 2010;21:482001.

42. Bunschoten A, van Willigen DM, Buckle T, et al. Tailoring fluorescent dyes to optimize a hybrid RGD-tracer. *Bioconjug Chem.* 2016;27:1253-1258.

43. Baranski AC, Schafer M, Bauder-Wust U, et al. PSMA-11-derived dual-labeled PSMA inhibitors for preoperative PET imaging and precise fluorescence-guided surgery of prostate cancer. *J Nucl Med.* 2018;59:639-645.

44. Hensbergen AW, van Willigen DM, Welling MM, et al. Click Chemistry in the Design and Production of Hybrid Tracers. *ACS Omega.* 2019;4:12438-12448.

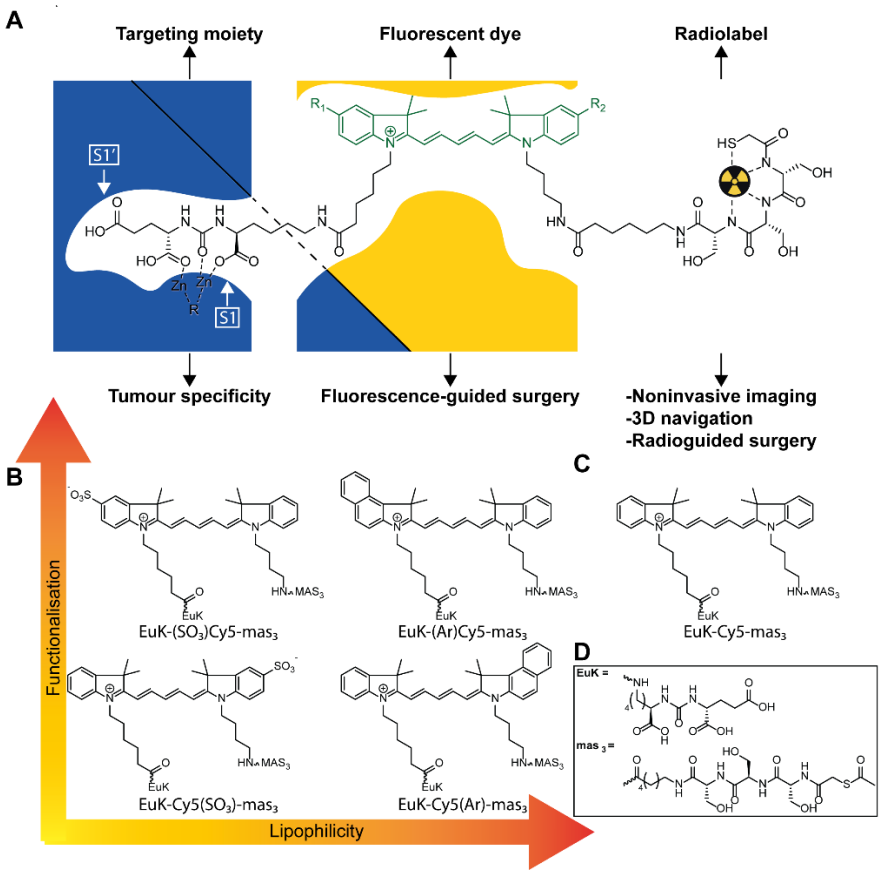

Figure 1. A) Schematic overview of the working hypothesis, exemplified by a hybrid tracer inside the PSMA binding site with interactions between the dye and the amphipathic funnel B) Selected hybrid tracers with functionalisation introduced on the indole with different lipophilicities. C) Hybrid tracer based on "control" Cy5 dye. D) chemical structures of EuK and 2-mercaptoacetyl-seryl-seryl-seryl (mas_3) moieties.

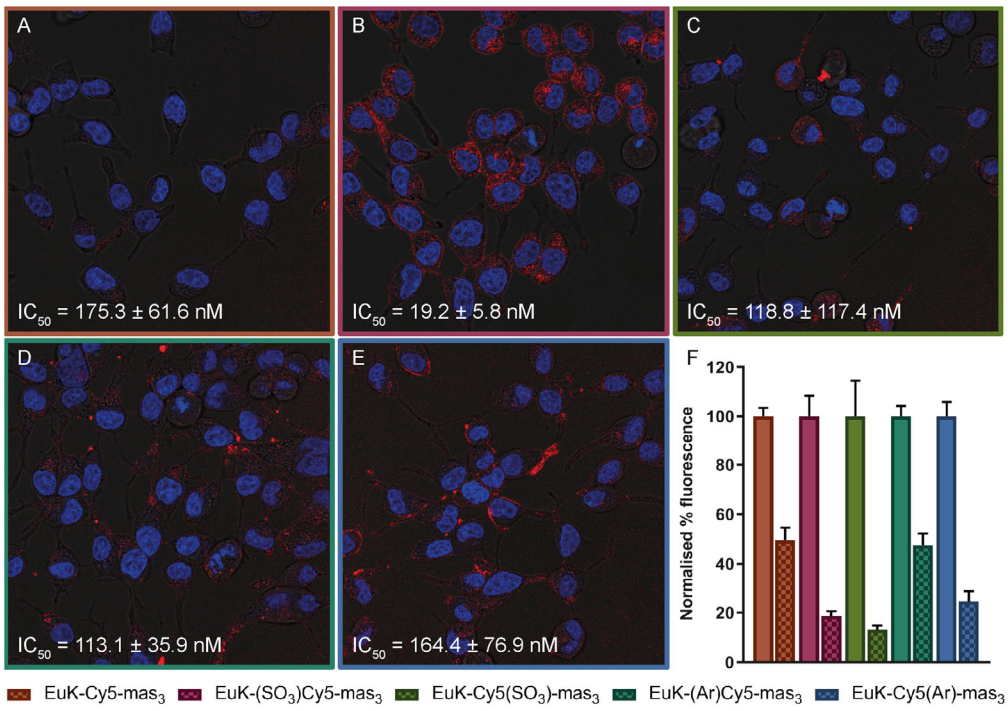

Figure 2. *In vitro* assessment of hybrid tracers. Staining of the extracellular expression of the PSMA on C2-2B$_4$ cells after incubation with nuclear staining (Hoechst; in blue) and a hybrid tracer (Cy5; in red) with IC_{50} values (measured with ^{125}I-EuK–I-BA as competitive radioligand). A) EuK-Cy5-mas$_3$; or B) EuK-(SO$_3$)Cy5-mas$_3$; or C) EuK-Cy5(SO$_3$)-mas$_3$; or D) EuK-(Ar)Cy5-mas$_3$; or E) EuK-Cy5(Ar)-mas$_3$; F) blocking (chequered) of the PSMA with EuK–I-BA. Binding affinity values represented as mean ± SD; *p* values are reported as **** = $p \leq 0.0001$.

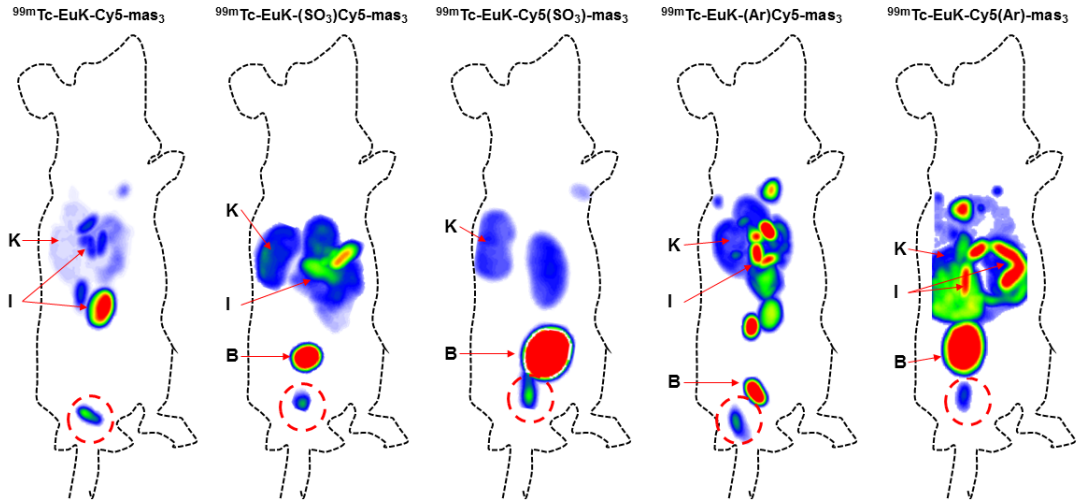

Figure 3. *In vivo* SPECT imaging evaluation using BALB/c nude mice with orthotopically transplanted PC346C cells injected with either one of the PSMA hybrid tracer analogues. All images are scaled relative to the tumour. K = kidneys, I = intestines and B = bladder; tumor encircled in red

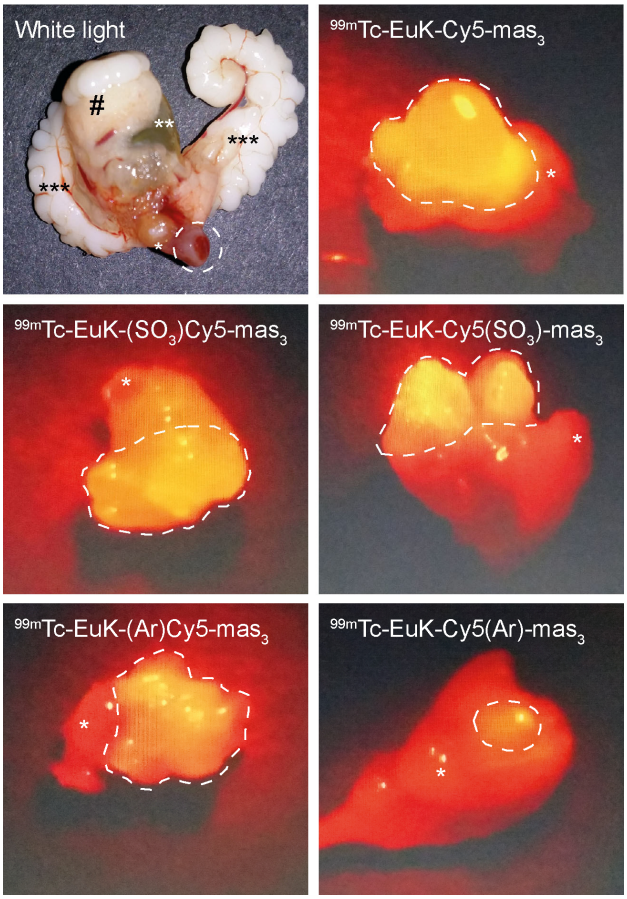

Figure 4. White light and *ex vivo* fluorescence imaging of tumour-containing prostate tissue (*),the bladder (**), the seminal vesicles (***) and abdominal adipose tissue (#) after injection of corresponding hybrid tracer.

Table 1. (Photo)physical characteristics of PSMA-targeting hybrid tracers.

Compound	$\lambda_{ex,max}/\lambda_{em,max}$ in H_2O/PBS (Stokes shift; nm)	Φ_F (% in PBS)	Brightness ($\cdot 10^4$ $M^{-1} \cdot cm^{-1}$ in PBS)	Lipophilicity ($logP_{(o/w)}$; n = 6)*	Plasma protein binding (n = 3)	Serum stability after 24 h (% remaining; absorbance/fluorescence; n = 2)
EuK-Cy5-mas$_3$	644/663 (18)	12	1.1†	-2.13 ± 0.10	88.3 ± 1.6	80 ± 6/86 ± 5
EuK-(SO$_3$)Cy5-mas$_3$	648/664 (16)	15	1.4†	-2.86 ± 0.05	85.0 ± 2.3	97 ± 2/89 ± 6
EuK-Cy5(SO$_3$)-mas$_3$	648/664 (16)	10	1.5†	-2.70 ± 0.01	87.4 ± 2.0	82 ± 7/85 ± 1
EuK-(Ar)Cy5-mas$_3$	664/682 (18)	9	0.3†	-1.75 ± 0.10	90.7 ± 1.3	85 ± 3/79 ± 1
EuK-Cy5(Ar)-mas$_3$	663/680 (17)	12	0.7†	-1.84 ± 0.06	89.0 ± 2.5	75 ± 0/76 ± 0

*Measured using ^{99m}Tc-labeled hybrid tracers †Calculated using the molecular extinction coefficient of the free fluorophore

Hybrid Tracers Based on Cyanine Backbones Targeting Prostate-Specific Membrane Antigen – Tuning Pharmacokinetic Properties and Exploring Dye–Protein Interaction

Supplemental Information

Albertus W. Hensbergen,[1] Tessa Buckle,[1] Danny M. van Willigen,[1] Margret Schottelius,[2] Mick M. Welling,[1] Felicia A. van der Wijk,[1] Tobias Maurer,[3] Henk G. van der Poel,[4] Gabri van der Pluijm,[5] Wytske M. van Weerden,[6] Hans-Jürgen Wester,[2] Fijs W. B. van Leeuwen[1,*]

[1]Interventional Molecular Imaging Laboratory, Department of Radiology, Leiden University Medical Center, Leiden, The Netherlands

[2]Pharmazeutische Radiochemie, Technische Universität München, Garching, Germany

[3]Martini-Klinik, Universitätsklinikum Hamburg-Eppendorf, Hamburg, Germany

[4]Department of Urology, Netherlands Cancer Institute-Antoni van Leeuwenhoek Hospital, Amsterdam, The Netherlands

[5]Department of Urology, Leiden University Medical Centre, Leiden, The Netherlands

[6]Department of Urology, Erasmus MC Cancer Institute, Erasmus University Medical Center, Rotterdam, The Netherlands

[*]Corresponding author: Fijs W. B. van Leeuwen. Interventional Molecular Imaging Laboratory, Department of Radiology, Leiden University Medical Center, Albinusdreef 2, 2333 ZA Leiden, The Netherlands. Phone: +31715266029. E-mail: f.w.b.van_leeuwen@lumc.nl

Materials and Methods

Synthesis

General

All chemicals and solvents were obtained from commercial sources and used without further purification. DMF and DCM used were dried with 4Å molecular sieves, unless stated otherwise. Column chromatography was performed with 40–63 µm silica (Silicycle). Dry column vacuum chromatography was performed as published by Pedersen *et al*. (*1*) with 15–40 µm silica (Merck) and Hyflo Supercell Celite (Sigma-Aldrich). HPLC was performed a Waters HPLC system using either a 1525EF or 2545 pump and a 2489 UV/VIS detector. For preparative HPLC either a Dr. Maisch GmbH Reprosil-Pur 120 C18-AQ 10 µm (250 × 20 mm) column or a XBridge Prep C8 10µm OBD 30x250mm column was used with a gradient of 0.1% TFA in H_2O/CH_3CN 95:5 to 0.1% TFA in H_2O/CH_3CN 5:95 in 40 minutes (12 or 25 mL/min, respectively) was employed. For semi-preparative HPLC a Dr. Maisch GmbH Reprosil-Pur C18-AQ 10 µm (250 × 10 mm) column was used and a gradient of 0.1% TFA in H_2O/CH_3CN 95:5 to 0.1% TFA in H_2O/CH_3CN 5:95 in 40 minutes (5 mL/min) was employed. For analytical HPLC a Dr. Maisch GmbH Reprosil-Pur C18-AQ 5 µm (250 × 4.6 mm) column was used and a gradient of 0.1% TFA in H_2O/CH_3CN 95:5 to 0.1% TFA in H_2O/CH_3CN 5:95 in 40 minutes (1 mL/min) was employed. Mass spectrometry was performed on a Bruker Microflex MALDI-TOF.

Merrifield resin synthesis

As performed by Lopalco *et al*. (2) Chloromethyl polystyrene resin (8.3 g, 15.0 mmol), N-Boc-aminophenol (9,4 g, 45.0 mmol), TBAI (1,7 g, 4.5 mmol) and $CsCO_3$ (14.7, 45.0 mmol) were dissolved in acetone, refluxed at 70 °C overnight under nitrogen atmosphere. Resin was then washed extensively with 100 mL DMF, H_2O, DMF, DCM and Et_2O and dried *in vacuo*. 4-(4-nitrobenzyl)pyridine test was used to determine reaction completion. 10.3 g (90% isolated yield) of Merrifield resin was formed.

(7R,10R,13R)-7,10,13-tris(hydroxymethyl)-2,5,8,11,14-pentaoxo-3-thia-6,9,12,15-tetraazahenicosan-21-oic acid (mas_3-Ahx-COOH)

mas_3-Ahx-COOH (1 mmol) was synthesised using standard (Fmoc) solid phase synthesis. After completion of the on-resin compound, it was cleaved by stirring in TFA for 3 h. The solution was drained and the solvent was evaporated *in vacuo*, re-dissolved in tBuOH/H_2O (1:1) and lyophilised. Lyophilisation yielded the title compound as a white, fluffy solid m/z $[M+Na]^+$ calcd. 531.532, found 530.998. The solid was used without further purification.

2,5-dioxopyrrolidin-1-yl (7R,10R,13R)-7,10,13-tris(hydroxymethyl)-2,5,8,11,14-pentaoxo-3-thia-6,9,12,15-tetraazahenicosan-21-oate (mas_3-Ahx-COOSu)

mas_3-Ahx-COOH (100 mg, 196.85 µmol) was dissolved in dry DMSO (2.5 mL) after which HSPyU (162 mg, 393.70 µmol) and DiPEA (171 µL, 984.25 µmol) were added. The solution was stirred under a N_2 atmosphere at room temperature for 30 minutes after which ethyl acetate (50 mL) was added. After centrifugation the supernatant was decanted and the white precipitate was washed 3 times with ethyl acetate (50 mL) and one time with diethyl ether (50 mL). The remaining solid was desiccated and purified by preparative HPLC. The correct fractions were pooled and lyophilised giving the title compound as a white solid in a 34% isolated yield (40 mg).

OtBu-Glu(OtBu)-urea-Lys(Z)-OtBu (EuK(tBu)$_3$-Z)

OtBu-Glu(OtBu)-urea-Lys(Z)-OtBu was synthesised as inspired by Khan *et al.* (3) H-Glu(OtBu)-OtBu.HCl (1.0 g, 3.38 mmol), 4-nitrophenyl chloroformate (682 mg, 3.38 mmol) and triethylamine (943 µL, 6.76 mmol) were dissolved in dry DCM (20 ml). The mixture was refluxed under a N_2 atmosphere for 25 minutes followed by stirring at r.t. for 60 minutes. A white precipitate was formed which disappeared when H-Lys(Z)-OtBu.HCl (1387 mg, 3.72 mmol) and triethylamine (943 µL, 6.76 mmol) were added. The solution turned yellow and was refluxed for 10 minutes before stirring at r.t. for 90 minutes. TLC showed full conversion of the starting material and thus the mixture was concentrated *in vacuo* to a small volume. Ethyl acetate (80 ml) was added and the suspension was stirred for 16 hours at r.t. after which it was filtered using a glass filter (P3). The white precipitate was washed with ethyl acetate, the filtrate was

combined with the supernatant and concentrated *in vacuo* to obtain a yellow oil. Column chromatography was performed using a gradient of ethyl acetate/hexane 1:5 to 1:2 over 6 column volumes, followed by 100% ethyl acetate for 1 column volume. The correct fractions were pooled and lyophilisation yielded the title compound as a slightly yellow oil in a 86% isolated yield (1.9 g, 95% pure). m/z $[M+Na]^+$ calcd. 644.8, found 644.6.

OtBu-Glu(OtBu)-urea-Lys(NH_2)-OtBu (EuK(tBu)$_3$-NH_2)

OtBu-Glu(OtBu)-urea-Lys(NH_2)-OtBu was synthesised inspired Makowski *et al.* (4) OtBu-Glu(OtBu)-urea-Lys(Z)-OtBu (1.9 g, 3.06 mmol), ammonium formate (385 mg, 6.11 mmol) and Pd/C (19 mg) were refluxed (100°C) in absolute ethanol (40 ml) under a N_2 atmosphere for 120 minutes. The reaction mixture was allowed to cool down to r.t. before filtering the suspension over Celite. The Celite was subsequently rinsed with absolute ethanol (50 ml). The solvent was removed *in vacuo* resulting in a yellow oil. Purification by HPLC yielded the title compound in quantitative yield as a yellowish oil, (1.6 g, 94% pure). m/z $[M+H]^+$ calcd. 487.6, found 488.1 $[M+Na]^+$ calcd. 510.6, found 510.2. The oil was diluted with dry methanol for further use (94 mg/mL).

The (sulfo)indole-based building blocks for the Cy5-dyes were synthesised according to adjusted synthesis methods inspired by published procedures.(*5-7*) All products were directly used without further purification.

3-(4-(1,3-dioxoisoindolin-2-yl)butyl)-1,1-dimethyl-1H-benzo[e]indol-3-ium

1,1,2-trimethyl-1*H*-benzo[e]indole (6.3 g, 30 mmol) and 1-(4-bromobutyl)pyrrolidine-2,5-dione (25.4 g, 28.7 mmol) were added to sulfolane (60 mL) and stirred at 90 °C for 72 h under a N_2 atmosphere. The reaction mixture was precipitated in EtOAc and the resulting suspension was filtered. The residue was washed twice with Et_2O and EtOAc. Removing solvents *in vacuo* yielded a grey solid (9.2 g) which was used without any further purification.

6-(1,1-dimethyl-1,2-dihydro-3H-benzo[e]indol-3-yl)hexanoic acid

1,1,2-trimethyl-1*H*-benzo[e]indole (6.5 g, 31 mmol) and 6-bromohexanoic acid (12.1 g, 62 mmol) were heated at 70–95 °C in MeCN (60.0 mL) for 72 h under a N_2 atmosphere. The grey, solid product was washed twice with MeCN, Et_2O and EtOAc. Residual solvents were removed *in vacuo*, yielding a grey solid (6.6 g) that was used without further purification.

Synthesis of phthalimide dyes (general procedure A) (1a–1f)

As previously described (2). In short, the hemicyanine was prepared by heating the indole-based building block with N-((1E,3E)-3-(phenylimino)prop-1-en-1-yl)aniline in a mixture of AcOH/Ac_2O (1:1) to 90 °Covernight followed by stirring at 120 °C for 2 h. When the reaction was finished as determined by using UV/Vis spectroscopy (product at λ_{max} ~450 nm and starting material at λ_{max} ~390 nm), the mixture was cooled down and precipitated in diethyl ether. After repeated centrifugation, decanting and washing steps with diethyl ether and EtOAc the solid was dissolved in a 1:1 DCM/DMF mixture and directly added to the deprotected resin. The suspension was agitated at r.t. for 1 h. After this time, by-products were washed away with DCM/DMF mixtures and the cyanine dye was prepared by adding the corresponding second indole-based building block in a mixture of pyridine/Ac_2O (3:1). This mixture was agitated at r.t. for 18 h. Crude dyes were purified by means of DCVC (EtOAc/MeOH) and subsequent preparative HPLC.

Phth-Cy5-COOH (**1a**)

2-((1E,3E)-5-((E)-1-(5-carboxypentyl)-3,3-dimethylindolin-2-ylidene)penta-1,3-dien-1-yl)-1-(4-(1,3-dioxoisoindolin-2-yl)butyl)-3,3-dimethyl-3H-indol-1-ium was obtained from 1-(4-(1,3-dioxoisoindolin-2-yl)butyl)-2,3,3-trimethyl-3H-indol-1-ium (220 mg, 0.6 mmol), 1-(5-carboxypentyl)-2,3,3-trimethyl-3H-indol-1-ium (660 mg, 2.4 mmol) and N-((1E,3E)-3-(phenylimino)prop-1-en-1-yl)aniline (683 mg, 2.7 mmol) in 23% isolated yield (59 mg) as a blue, fluffy solid after lyophilisation. ^{1}H NMR (300 MHz, MeOD) δ 8.23 (td, J = 13.2, 6.7 Hz, 2H), 7.95–7.70 (m, 4H), 7.56–7.17 (m, 8H), 6.63 (t, J = 12.4 Hz, 1H), 6.31 (d, J = 13.6

Hz, 2H), 4.32–4.05 (m, 4H), 3.78 (t, J = 5.3 Hz, 2H), 2.35 (t, J = 7.2 Hz, 2H), 1.86 (s, J = 3.0 Hz, 6H), 1.73 (t, J = 7.6 Hz, 14H), 1.61–1.47 (m, 2H). m/z $[M]^+$ calcd. 670.873, found 670.295.

Phth-Cy5(SO_3)-COOH (**1b**)

(E)-1-(5-carboxypentyl)-2-((2E,4E)-5-(1-(4-(1,3-dioxoisoindolin-2-yl)butyl)-3,3-dimethyl-3H-indol-1-ium-2-yl)penta-2,4-dien-1-ylidene)-3,3-dimethylindoline-5-sulfonate was obtained from 1-(4-(1,3-dioxoisoindolin-2-yl)butyl)-2,3,3-trimethyl-3H-indol-1-ium (264 mg, 0.6 mmol), 1-(5-carboxypentyl)-2,3,3-trimethyl-3H-indol-1-ium-5-sulfonate (1100 mg, 2.4 mmol) and N-((1E,3E)-3-(phenylimino)prop-1-en-1-yl)aniline (678 mg, 2.6 mmol) in 13% isolated yield (65 mg) as a blue, fluffy solid after lyophilisation. δ 8.31 (td, *J* = 13.0, 8.4 Hz, 1H), 7.91 – 7.76 (m, 2H), 7.61 (dd, *J* = 13.4, 5.0 Hz, 1H), 7.41 (d, *J* = 4.0 Hz, 1H), 7.33 (d, *J* = 8.3 Hz, 1H), 7.29 – 7.22 (m, 1H), 6.55 (t, *J* = 12.4 Hz, 1H), 6.30 (dd, *J* = 18.1, 13.9 Hz, 1H), 4.11 (s, 2H), 3.62 (d, 11H), 2.20 (t, *J* = 7.2 Hz, 1H), 2.08 (s, 1H), 1.71 (s, 1H), 1.68 (d, *J* = 2.2 Hz, 5H), 1.61 – 1.49 (m, *J* = 14.6, 7.4 Hz, 1H), 1.44 – 1.33 (m, 1H), 1.28 (s, 1H), 1.23 (s, 1H), 1.14 (s, 1H), 0.87 (dd, *J* = 9.3, 5.5 Hz, 1H). m/z $[M+H]^+$ calcd. 750.930, found 750.600.

Phth-(SO_3)Cy5-COOH (**1c**)

2-((1E,3E)-5-((E)-1-(5-carboxypentyl)-3,3-dimethylindolin-2-ylidene)penta-1,3-dien-1-yl)-1-(4-(1,3-dioxoisoindolin-2-yl)butyl)-3,3-dimethyl-3H-indol-1-ium-5-sulfonate was obtained from 1-(4-(1,3-dioxoisoindolin-2-yl)butyl)-2,3,3-trimethyl-3H-indol-1-ium-5-sulfonate (440 mg, 1.0 mmol), 1-(5-carboxypentyl)-2,3,3-trimethyl-3H-indol-1-ium (1100 mg, 4.0 mmol) and N-((1E,3E)-3-(phenylimino)prop-1-en-1-yl)aniline (1200 mg, 4.4 mmol) in 5% isolated yield (39 mg) as a blue, fluffy solid after lyophilisation. δ 8.31 (t, *J* = 13.3 Hz, 1H), 7.92 – 7.76 (m, 2H), 7.68 – 7.56 (m, 1H), 7.46 – 7.29 (m, 1H), 7.23 (td, 1H), 6.56 (t, *J* = 12.5 Hz, 1H), 6.31 (d, *J* = 13.7 Hz, 1H), 4.12 (d, *J* = 5.8 Hz, 2H), 3.63 (s, 1H), 2.21 (t, *J* = 7.1 Hz, 1H), 1.68 (d, *J* = 8.6 Hz, 7H), 1.55 (t, 1H), 1.38 (t, 1H), 1.26 (d, *J* = 14.9 Hz, 2H), 1.11 (s, 1H), 0.87 (dd, *J* = 9.0, 5.0 Hz, 1H). m/z $[M+H]^+$ calcd. 750.930, found 750.778.

Phth-(SO_3)Cy5(SO_3)-COOH (**1d**)

2-((1E,3E)-5-((E)-1-(5-carboxypentyl)-3,3-dimethyl-5-sulfonatoindolin-2-ylidene)penta-1,3-dien-1-yl)-1-(4-(1,3-dioxoisoindolin-2-yl)butyl)-3,3-dimethyl-3H-indol-1-ium-5-sulfonate was obtained from 1-(4-(1,3-dioxoisoindolin-2-yl)butyl)-2,3,3-trimethyl-3H-indol-1-ium-5-sulfonate (264 mg, 0.6 mmol), 1-(5-carboxypentyl)-2,3,3-trimethyl-3H-indol-1-ium-5-sulfonate (1.7 g, 4.8 mmol) and N-((1E,3E)-3-(phenylimino)prop-1-en-1-yl)aniline (1.4 g, 5.3 mmol) in 16% isolated yield (86 mg) as a blue, fluffy solid after lyophilisation. δ 8.33 (td, *J* = 12.9, 5.6 Hz, 1H), 7.90 – 7.77 (m, 3H), 7.62 (td, *J* = 8.2, 1.5 Hz, 1H), 7.34 (d, *J* = 8.3 Hz, 1H), 6.55 (t, *J* = 12.4 Hz, 1H), 6.30 (dd, *J* = 13.9, 8.9 Hz, 1H), 4.14 – 4.00 (m, 9H), 3.96 (s, 1H), 3.62 (s, 1H), 3.55 (s, 1H), 2.29 (t, *J* = 7.2 Hz, 1H), 2.20 (t, *J* = 7.1 Hz, 1H), 2.08 (s, 1H), 1.68 (d, *J* = 5.4 Hz, 9H), 1.56 (dd, *J* = 14.9, 7.7 Hz, 1H), 1.38 (d, *J* = 6.4 Hz, 1H), 1.23 (s, 1H). m/z $[M+2H]^+$ calcd. 830.987, found 830.642.

Deprotection of the phthalimide (general procedure B) (2a–2f)

Compound **1a**–**1f** was dissolved in a solution of methylamine in EtOH (33 wt%) before stirring at r.t. for 4–7 hours. After completion, EtOH and residual methylamine were removed *in vacuo*. The crude was dissolved in H_2O/CH_3CN/TFA (75:25:0.1; 4.0 mL) and purified by preparative HPLC using a gradient of H_2O/CH_3CN/ TFA 75:25:0.1 to H_2O/CH_3CN/TFA 10:90:0.1 in 50 min.

2-((1E,3E)-5-((E)-1-(4-aminobutyl)-3,3-dimethylindolin-2-ylidene)penta-1,3-dien-1-yl)-1-(5-carboxypentyl)-3,3-dimethyl-3H-indol-1-ium (**2a**). Blue, fluffy solid after lyophilisation, 59% isolated yield. m/z $[M]^+$ calcd. 540.771, found 540.600.

2-((1E,3E)-5-((E)-1-(4-aminobutyl)-3,3-dimethylindolin-2-ylidene)penta-1,3-dien-1-yl)-1-(5-carboxypentyl)-3,3-dimethyl-3H-indol-1-ium-5-sulfonate (**2b**). Blue, fluffy solid after lyophilisation, used without further purification. m/z $[M+H]^+$ calcd. 620.828, found 620.570.

(E)-1-(4-aminobutyl)-2-((2E,4E)-5-(1-(5-carboxypentyl)-3,3-dimethyl-3H-indol-1-ium-2-yl)penta-2,4-dien-1-ylidene)-3,3-dimethylindoline-5-sulfonate (**2c**). Blue, fluffy solid after lyophilisation, 21% isolated yield. m/z $[M+H]^+$ calcd. 620.828, found 620.400.

2-((1E,3E)-5-((E)-1-(4-aminobutyl)-3,3-dimethylindolin-2-ylidene)penta-1,3-dien-1-yl)-3-(5-carboxypentyl)-1,1-dimethyl-1H-benzo[e]indol-3-ium (**2d**). Blue, fluffy solid after lyophilisation, 60% isolated yield. m/z $[M+H]^+$ calcd. 590.831, found 590.372.

2-((1E,3E,5E)-5-(3-(4-aminobutyl)-1,1-dimethyl-1,3-dihydro-2H-benzo[e]indol-2-ylidene)penta-1,3-dien-1-yl)-1-(5-carboxypentyl)-3,3-dimethyl-3H-indol-1-ium (**2e**). Blue, fluffy solid after lyophilisation, 68% isolated yield. m/z $[M+H]^+$ calcd. 590.831, found 590.319.

2-((1E,3E,5E)-5-(3-(4-aminobutyl)-1,1-dimethyl-1,3-dihydro-2H-benzo[e]indol-2-ylidene)penta-1,3-dien-1-yl)-3-(5-carboxypentyl)-1,1-dimethyl-1H-benzo[e]indol-3-ium (**2f**). Blue, fluffy solid after lyophilisation, 76% isolated yield. m/z $[M+H]^+$ calcd. 640.891, found 640.451.

Coupling of the mas$_3$ chelate (general procedure C) (3a–3f)

The deprotected cyanine dye as prepared above (**2a**–**2f**) was dissolved in DMSO before basifying with DiPEA (3.0 eq) and a solution of mas$_3$-Ahx-COOSu in DMSO (1.0 eq, 20 mg/mL). The resulting mixture was stirred at r.t. for 60–90 minutes before adding DMSO (500 µL) and H_2O/TFA (99.9:0.1; 3.0 mL) and purifying by preparative HPLC using a gradient of H_2O/CH_3CN/TFA 75:25:0.1 to H_2O/CH_3CN/TFA 10:90:0.1 in 50 min.

(**3a**). Blue, fluffy solid after lyophilisation, used without any further purification. m/z $[M]^+$ calcd. 1030.532, found 1031.001.

(**3b**). Blue, fluffy solid after lyophilisation, used without further purification. m/z $[M+H]^+$ calcd. 1111.356, found 1111.086.

(**3c**). Blue, fluffy solid after lyophilisation, used without any further purification. m/z $[M+H]^+$ calcd. 1111.356, found 1111.539.

(**3d**). Blue, fluffy solid after lyophilisation, 77% isolated yield. m/z $[M]^+$ calcd. 1081.359, found 1081.188.

(**3e**). Blue, fluffy solid after lyophilisation, 57% isolated yield. m/z $[M]^+$ calcd. 1081.359, found 1081.501.

(**3f**). Blue, fluffy solid after lyophilisation, 71% isolated yield. m/z $[M]^+$ calcd. 1131.419, found 1131.094.

Coupling of the EuK(tBu)$_3$ moiety (general procedure D) (4a–4f)

3a–3f was dissolved in DMSO (1.0 mL) before adding PyBOP (4.0 eq) and NMM (2.0 eq). The resulting mixture was stirred at r.t. for 20 minutes before the addition of $EuK(tBu)_3$ (2.0 eq). This mixture was stirred at r.t. for 5–6 hours before adding H_2O/TFA (99.1:0.1; 3.0 mL) and where appropriate, the mixture was further acidified to pH = 1–3 with a few drops of TFA. The crude material was then purified by preparative HPLC using a gradient of H_2O/CH_3CN/ TFA 75:25:0.1 to H_2O/CH_3CN/TFA 10:90:0.1 in 50 min.

(**4a**). Blue, fluffy solid after lyophilisation, 89% isolated yield. m/z $[M]^+$ calcd. 1500.922, found 1500.995.

(**4b**). Blue, fluffy solid after lyophilisation, 35% isolated yield. m/z $[M+H]^+$ calcd. 1580.979, found 1580.529.

(**4c**). Blue, fluffy solid after lyophilisation, 56% isolated yield. m/z $[M+H]^+$ calcd. 1580.979, found 1580.829.

(**4d**). Blue, fluffy solid after lyophilisation, 56% isolated yield. m/z $[M]^+$ calcd. 1550.982, found 1151.119.

(**4e**). Blue, fluffy solid after lyophilisation, 67% isolated yield. m/z $[M]^+$ calcd. 1550.982, found 1551.559.

(**4f**). Blue, fluffy solid after lyophilisation, 57% isolated yield. m/z $[M]^+$ calcd. 1601.042, found 1600.914.

Deprotection of the EuK moiety (general procedure E) (5a–5f)

4a–**4f** was dissolved in a solution of TFA/triisopropylsilane (95:5; 1.5 mL) before stirring under a N_2 atmosphere for 3.5 hours. After this time, solvents were removed *in vacuo* and the resulting crude was then purified by preparative HPLC using a gradient of H_2O/CH_3CN/ TFA 75:25:0.1 to H_2O/CH_3CN/TFA 10:90:0.1 in 50 min.

(**5a; EuK-Cy5-mas$_3$**). Blue, fluffy solid after lyophilisation, 61% isolated yield, 99% pure as assessed by HPLC. m/z $[M]^+$ calcd. 1332.598, found 1332.439.

(**5b; EuK-(SO$_3$)Cy5-mas$_3$**). Blue, fluffy solid after lyophilisation, 18% isolated yield. m/z $[M+H]^+$ calcd. 1412.655, found 1412.528.

(**5c; EuK-Cy5(SO$_3$)-mas$_3$**). Blue, fluffy solid after lyophilisation, 28% isolated yield. m/z $[M+H]^+$ calcd. 1412.655, found 1412.461.

(**5d; EuK-(Ar)Cy5-mas$_3$**). Blue, fluffy solid after lyophilisation, 63% isolated yield, 98% pure as assessed by HPLC. m/z $[M+H]^+$ calcd. 1382.658, found 1382.526.

(**5e; EuK-Cy5(Ar)-mas$_3$**). Blue, fluffy solid after lyophilisation, 98% isolated yield, 97% pure as assessed by HPLC. m/z $[M+H]^+$ calcd. 1382.658, found 1382.388.

(**5f; EuK-(Ar)Cy5(Ar)-mas$_3$**). Blue, fluffy solid after lyophilisation, 73% isolated yield, 98% pure as assessed by HPLC. m/z $[M+H]^+$ calcd. 1432.718, found 1432.544.

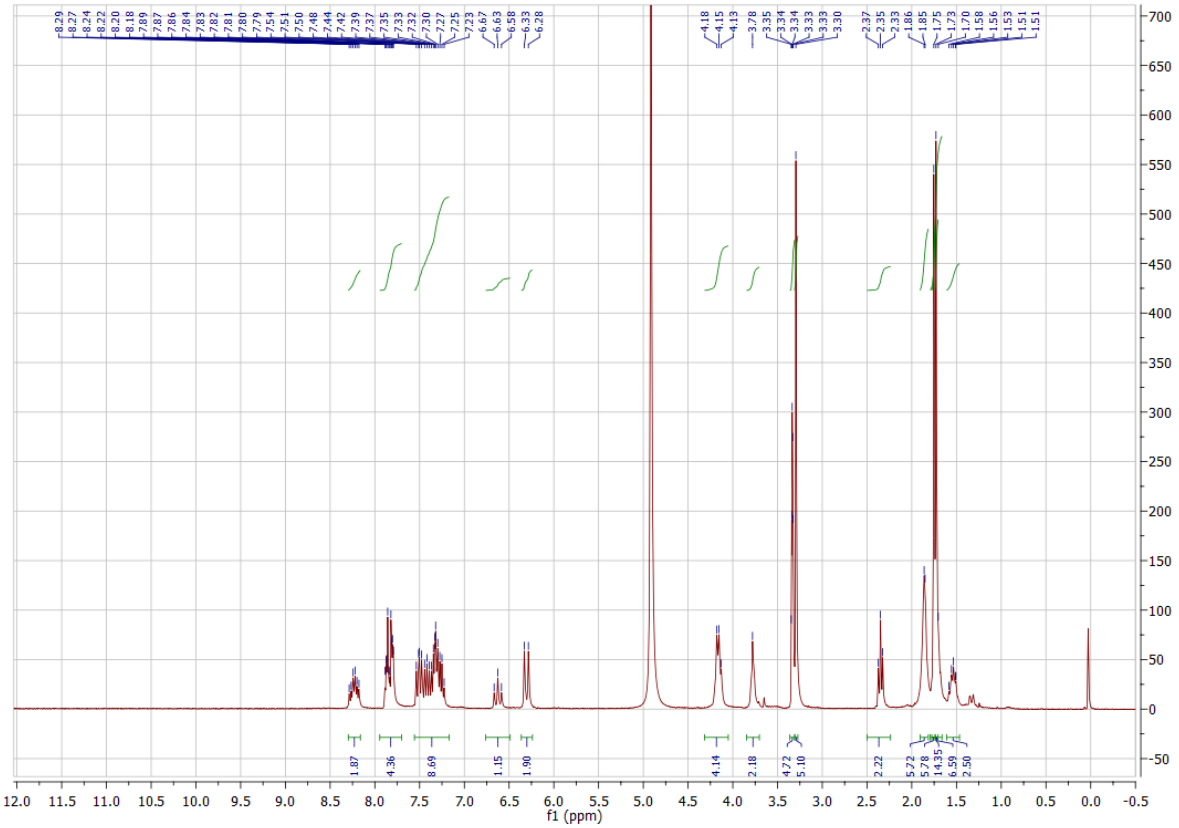

Supplemental Figure 1. ^{1}H NMR spectrum of Phth-Cy5-COOH (**1a**)

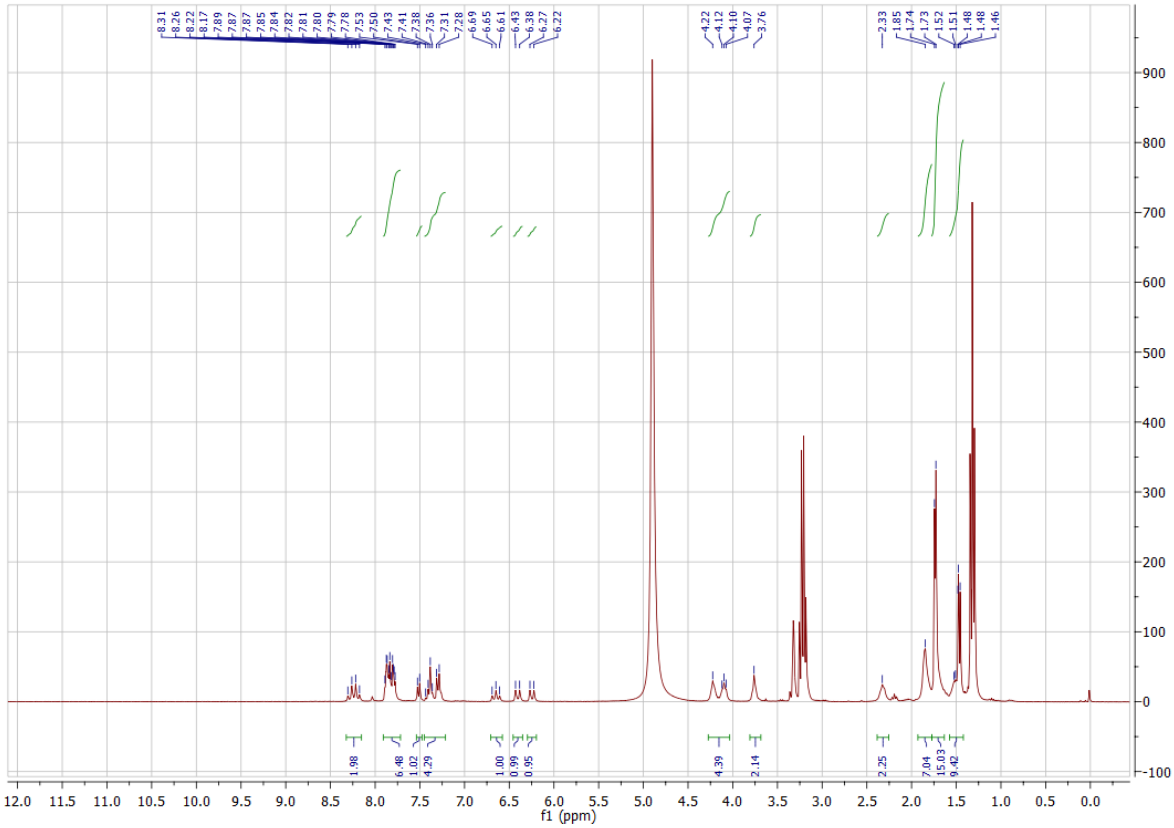

Supplemental Figure 2. ^{1}H NMR of Phth-Cy5-(SO_3)COOH (**1b**)

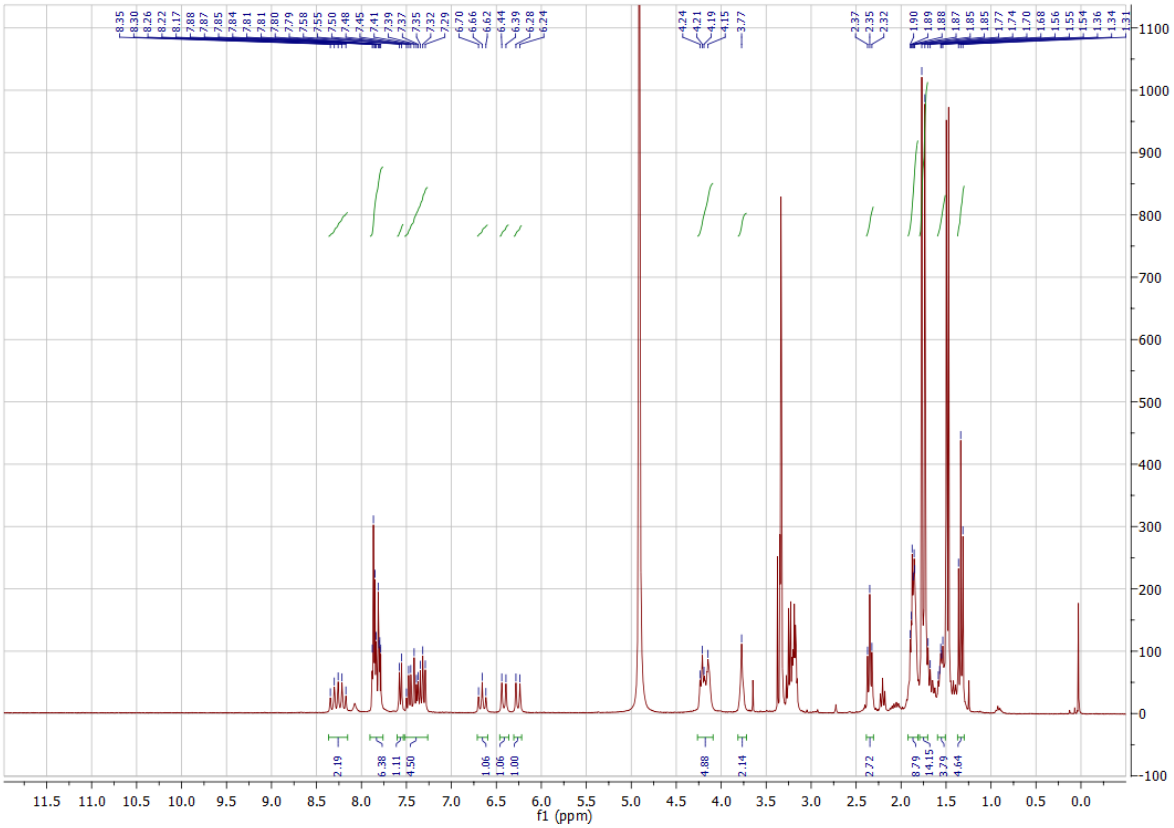

Supplemental Figure 3. ^{1}H NMR of Phth-(SO_3)Cy5-COOH (**1c**)

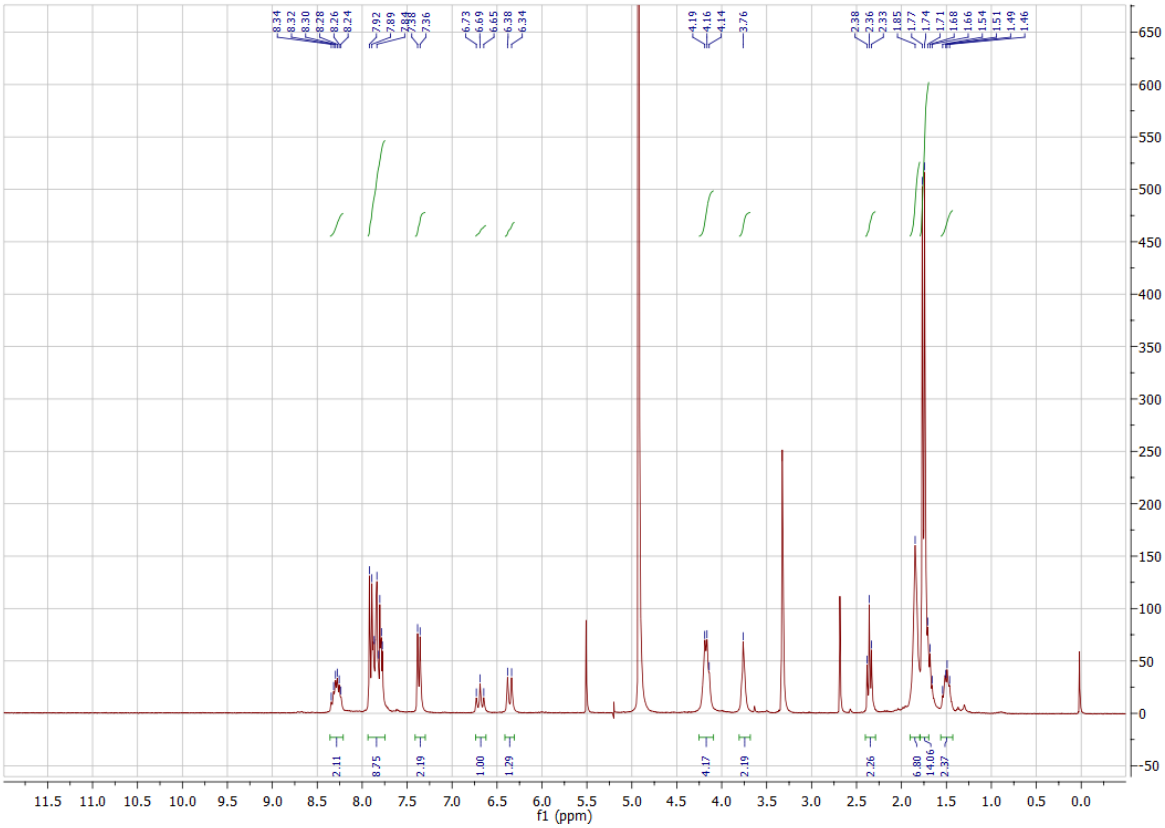

Supplemental Figure 4. ^{1}H NMR of Phth-(SO_3)Cy5-(SO_3)COOH (**1d**)

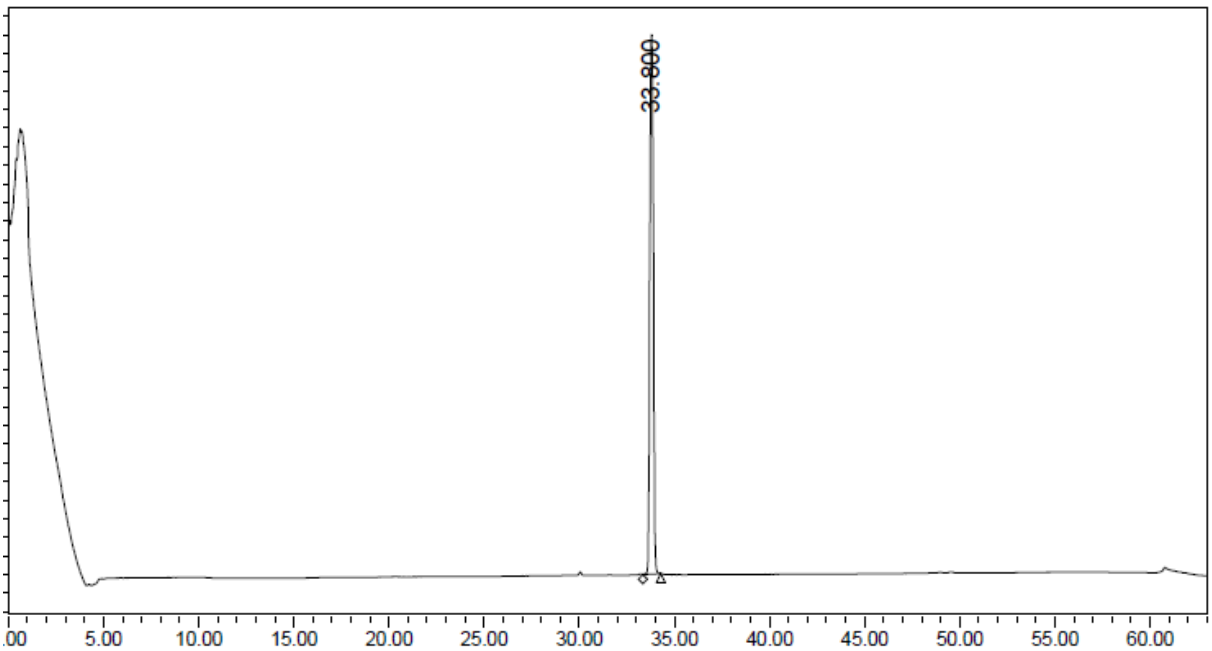

Supplemental Figure 5. Chromatogram (650 nm) of EuK-Cy5-mas$_3$

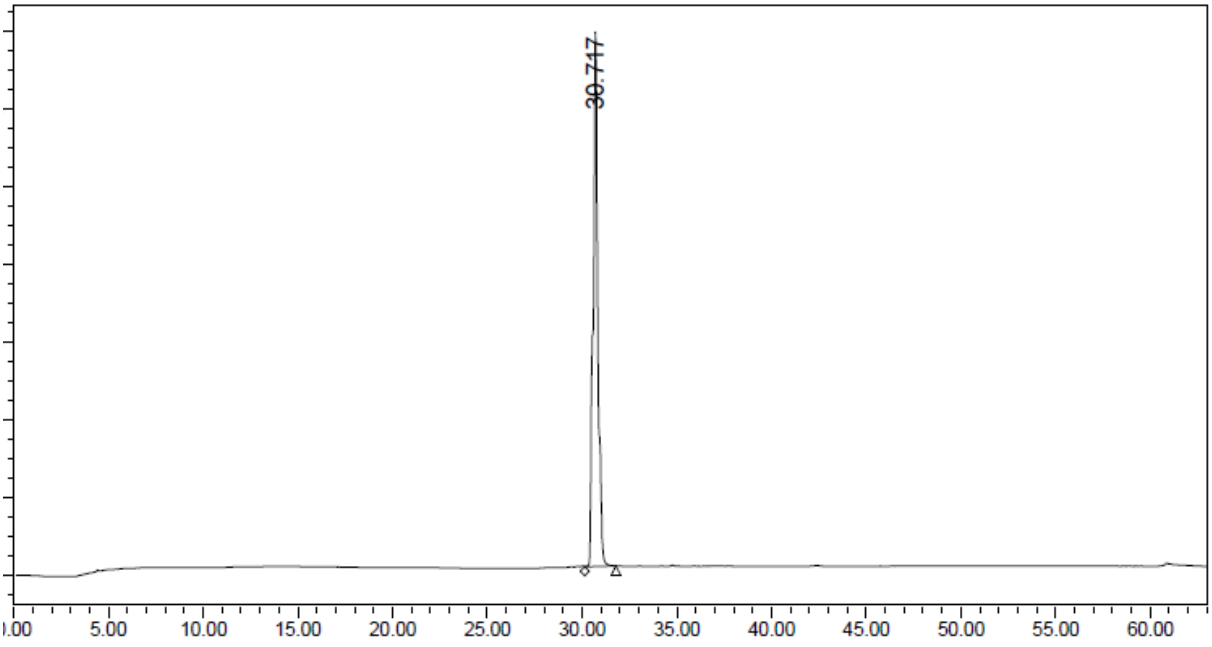

Supplemental Figure 6. Chromatogram (650 nm) of EuK-(SO_3)Cy5-mas_3

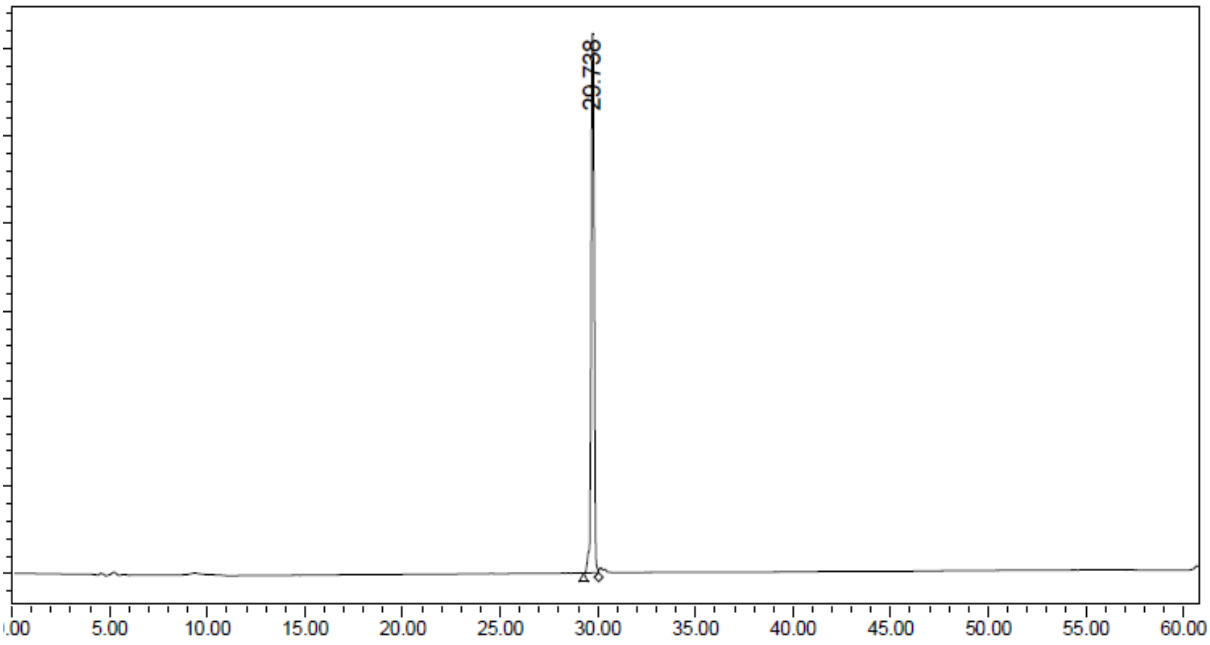

Supplemental Figure 7. Chromatogram (650 nm) of EuK-Cy5(SO_3)-mas_3

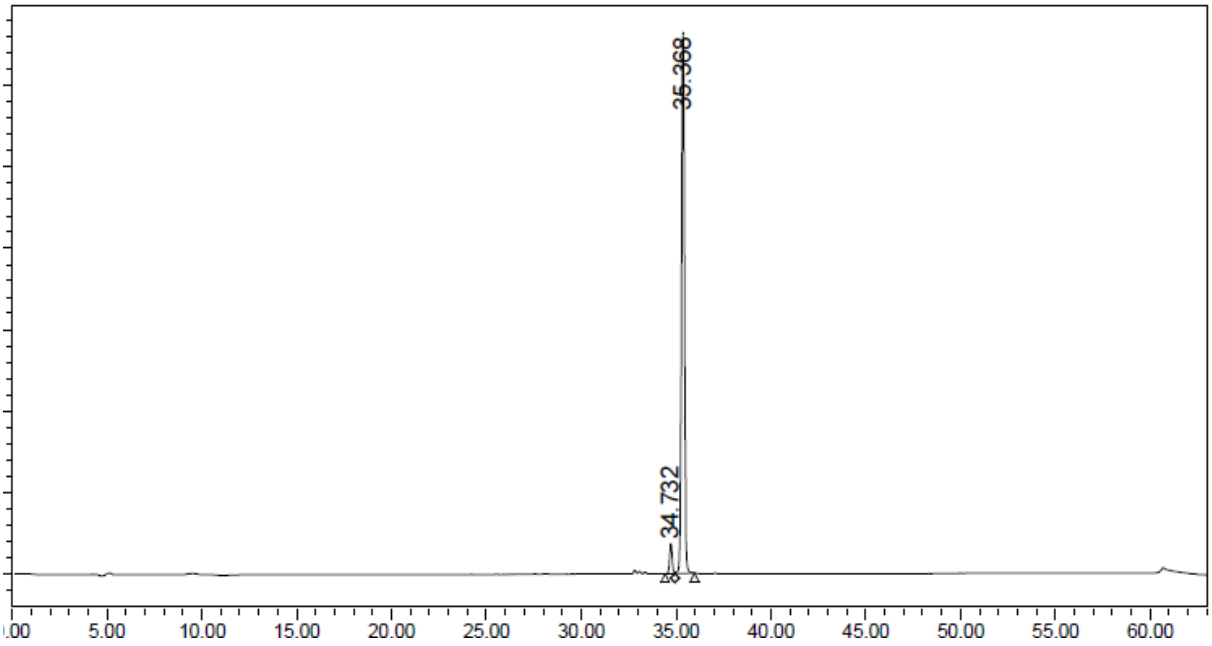

Supplemental Figure 8. Chromatogram (650 nm) of EuK-(Ar)Cy5-mas$_3$

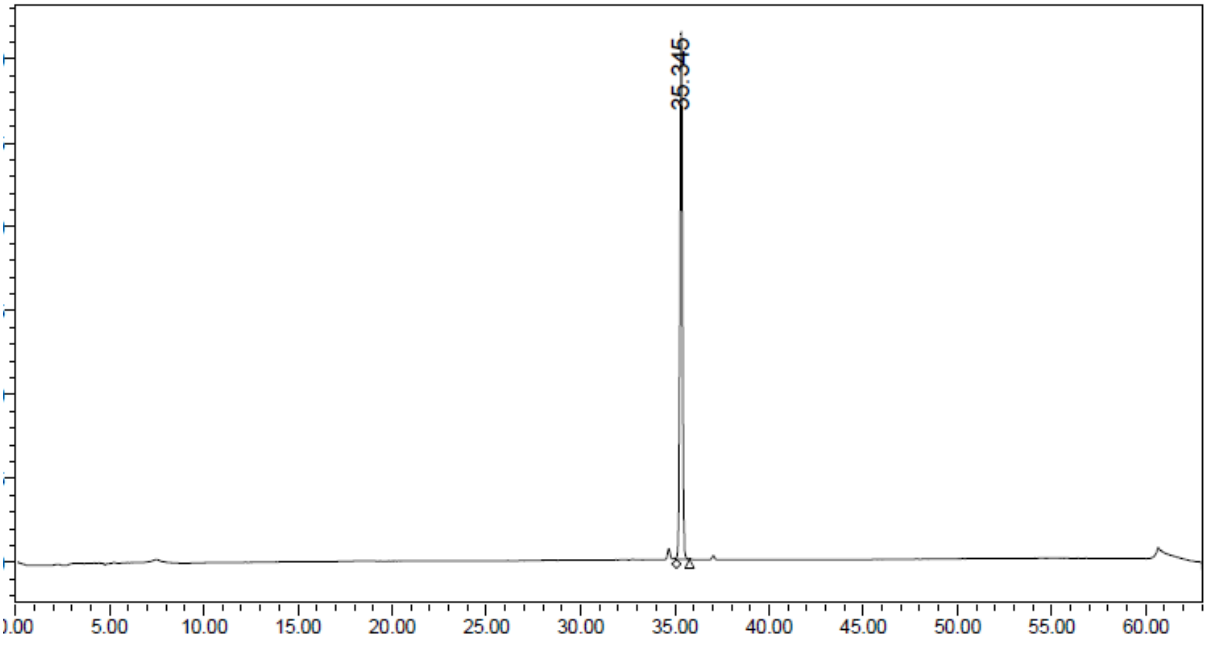

Supplemental Figure 9. Chromatogram (650 nm) of EuK-Cy5(Ar)-mas$_3$

Photophysical properties

Photophysical properties (ε, Φ_F and $\lambda_{ex}/\lambda_{em}$) were assessed as based on earlier published procedures (*8,9*).

Molar extinction coefficient (ε)

Stock solutions in DMSO-d_6 were diluted in DMSO, H2O or PBS to obtain a concentration range of 7.5-0.25 µM in triplo in all solvents. Optical density was measured at t = 10 min after preparation and the plotted absorbance was normalised for cuvette path length and concentration. The ε was then determined by applying a linear regression coefficient.

Brightness

The ε of the hybrid tracers could not be determined due their large molecular size. Therefore, the brightness of each hybrid tracer was calculated by multiplying its quantum yield (Φ_F) by the epsilon of the corresponding free fluorophore (Table SI1)

Radiochemistry

The hybrid tracers were radiolabelled with ^{99m}Tc for lipophilicity and *in vivo* experiments as follows:

3.90 µL (6 nmol) of a 1.54 mM hybrid tracer solution was mixed with 8.13 µL of 0.5M phosphate buffer pH 8, 12.03 µL of 0.25M phosphate buffer pH 8, 9.62 µL of a 250 mg/mL sodium L-tartrate solution in 0.5M phosphate buffer pH 8, 2.41 µL of 4 mg/mL stannous(II)chloride solution (freshly made and purged with He) in a 3 mg/mL L-ascorbic acid solution, in which the latter was prepared in a 10mM HCl solution. After addition of 240 MBq of ^{99m}Tc in saline, the solution was heated to 90-95 °C in capped vials for 20-30 minutes. Then the caps were removed and the solutions were cooled to room temperature for 10 minutes. The degree of labelling (about 95%) was determined by RP-TLC using an eluent of CH_3CN:H_2O (3:7) and used without further purification.

Lipophilicity

The lipophilicity ($logP_{(o/w)}$) was determined based on previously published methods.(*10*) In short, 1-octanol (500 µL) was added to a 14.6 ± 0.2 µM solution of hybrid tracer in PBS (500 µL) in a 2 mL Eppendorf tube (n=6). The tubes were vortexed at maximum speed using an IKA Vibrofix VF1 (IKA®-Werke GmbH & Co. KG, Staufen, Germany) for 3 minutes and consecutively centrifuged for 5 minutes at 6.000 *g* in an Eppendorf 5415D centrifuge (Eppendorf, Hamburg, Germany) to achieve quantitative phase separation. Hereafter, 300 µL of the organic or aqueous phase was transferred to individual Eppendorf tubes. PBS (300 µL) and ethanol (600 µL) were added to the organic phase followed by vortexing for 5 seconds. 1-octanol (300 µL) and ethanol (600 µL) were added to the aqueous phase followed by vortexing for 5 seconds. 1 mL of each sample (total 12 per compound) was transferred to a disposable cuvette and measured using fluorescence spectrometry in a Perkin Elmer LS55 (Perkin Elmer, Waltham, USA).

Plasma protein binding

Plasma protein binding was determined based on methods as previously published using an 8K Rapid Equilibrium Dialysis plate (Sigma Aldrich, Prod #90006) (*8*). In short, 297 µL of FCS (fetal calf serum, heat inactivated) was added to the dialysis chamber (n=2) and 550 µL of PBS was added to the reservoir chamber (n=2). As a control (n=1), 300 µL of PBS was added to the dialysis chamber and 547 µL of FCS was added to the reservoir chamber. 3 µL of a 100 µM hybrid tracer solution in PBS was added to the FCS-containing chambers. The plate was closed using sealing tape and subsequently incubated at r.t. on a Vibrax VXR orbital shaker (Ika, Staufen, Germany) at 200-250 rpm for 4 h, after which 100 µL aliquots were withdrawn from both chambers for each of the compounds. 100 µL phosphate buffer was then added to the aliquots containing FCS, and 100 µL FCS was added to the aliquots containing PBS. Fluorescence spectra were recorded using a Perkin Elmer LS55 (Perkin Elmer, Waltham, USA) and the percentage of compound bound to serum proteins was calculated as follows:

$$PPB\ (\%) = 100 \cdot \left(1 - \left(\frac{\sum fluorescence_{PBS}}{\sum fluorescence_{FCS}}\right)\right)$$

Plasma protein stability

The plasma protein stability was assessed using previously published methods (*11*). In short: four samples of each hybrid tracer (one for each individual time point) were created by incubating a 1 µM solution of each hybrid tracer in non-heat inactivated FBS at 37 °C in closed vials. After diluting the sample 1:1 with PBS at t = 0 and 24 h, their maximum absorbance and accumulated fluorescence were measured using a Amersham Ultrospec 2100 pro (Amersham Bioscience, Amersham, United Kingdom) and Perkin Elmer LS55 (Perkin Elmer, Waltham, USA), respectively.

Stability of the ^{99m}Tc-mas$_3$ complex at 24 h was carried out as previously described (10).

PSMA Affinity

Affinity of the different tracers for PSMA (IC_{50}) was assessed according to previously described methods by Weineisen *et al. (10)* In short, LNCaP cells were incubated with unlabelled hybrid tracer of interest in increasing concentration (10^{-10}–10^{-4} M in HBSS (1% BSA)) and (^{125}I-I-BA)EuK as competitive radioligand in HBSS (1% BSA). Experiments were carried out in triplicate for each concentration. The final radioligand concentration was 0.2 nM in all binding assays. Cells were incubated on ice for 60 min.

Protein-ligand docking

Protein–ligand docking interactions were carried out to understand the differences in the affinity findings and calculated using AutoDock Vina 1.1.2 (*12*) and visualised using UCSF Chimera 1.31.1 (*13*) using the ligand-free human glutamate carboxypeptidase II (pdb ID 2OOT). After preparing the protein for docking in UCSF Chimera, the ligand molecule was selected and docking interactions were calculated. The most viable docking model was selected using the ViewDock plugin.

Fluorescence Confocal Microscopy

C4-2B$_4$ human prostate cells were cultured in Roswell Park Memorial Institute 1640 medium (RPMI-1640)

enriched with 10% Foetal Bovine Serum and penicillin/streptomycin (all Life Technologies Inc.) and 1 µM Enzalutamide (SelleckChem, S1250). Cells were kept under standard culturing conditions. For fluorescence confocal imaging, cells were seeded on glass bottom culture dishes (MatTek corporation) and placed in the incubator overnight. Confocal imaging was performed on viable cells, using a SP8 WLL fluorescence confocal microscope (Leica) (*11*). Cells were incubated with 1 µM of EuK-Cy5-mas_3, EuK-(SO_3)Cy5-mas_3, EuK-Cy5(SO_3)-mas_3, EuK-(Ar)Cy5-mas_3, or EuK-Cy5(Ar)-mas_3 for 1 h at 37 °C and washed with PBS thrice. Prior to imaging the nuclei of the cells were stained with Hoechst 33342 (ThermoFisher Scientific). Sequential scanning settings were applied to visualise all fluorescent features; Cy5 (λ_{ex} 633 nm, λ_{em} 650–700 nm and Hoechst (λ_{ex} 405 nm, λ_{em} 420–470 nm). Fluorescence intensities were determined according to previously used methods.(*7*)

In Vivo SPECT Imaging and Quantitative Assessment Biodistribution

For biodistribution (n=4) and for single photon emission computed tomography (SPECT) imaging (n=2) approximately 40 MBq was injected intravenously. At 2 h post-injection, SPECT imaging was performed followed by *ex vivo* evaluation of the biodistribution (in total n=6 animals/tracer). Total-body imaging and data reconstruction of PC346C-tumour-bearing mice was performed on a U-SPECT scanner (MILabs, Utrecht, The Netherlands) according to previously described methods (*5,11*).

After imaging, animals were sacrificed by cervical dislocation and various tissues were resected, weighed and counted for radioactivity. Quantitative biodistribution measurements (percentage of the injected dose per gram of tissue (% ID/g) and tumour-to-background ratios ($\frac{\%\frac{ID}{g}tumour}{\%\frac{ID}{g}background}$) were calculated.

In Vivo Tumour Model

PC346C cells were washed with HBSS and suspended in a mixture of HBSS (Invitrogen, Carlsbad, USA) and

Matrigel (VWR, Darmstadt, Germany) (1:1) prior to injection. Prepared PC346C cells (*14*) were orthotopically transplanted into the prostate of male BALB/c nude mice (Harlan; 6–8 weeks of age). Prior to transplantation, mice were anesthetised using a Hypnorm (VetaPharma Ltd.)/Dormicum (Midazolam; Roche)/H_2O solution (1:1:2; 5 μL/g i.p.). The prostate was located *via* a small incision in the abdominal wall whereafter 2.0 x 10^6 PC346C cells (in 20 µl; 1:1 HBSS/Matrigel) were injected into the prostate. After repositioning of the prostate, the incision was closed and pain relief was given via subcutaneous injection of 10 µL Temgesic (Buprenorphine, 5mg/ml, Actavis) in 0.5 mL 0.90% w/v of NaCl in H_2O, at 30 min prior to and 24 h after the procedure. Approximately 2 weeks after transplantation, palpable lesions were deemed suitable for further experiments when 2–5 mm in diameter. All animal experiments were approved by the local ethics committee of the LUMC prior to execution. Experiments were performed in accordance with the Experiments on Animals Act (Wod, 2014), the applicable legislation in the Netherlands in accordance with the European guidelines (EU directive no. 2010/63/EU) regarding the protection of animals used for scientific purposes. All experiments were executed in a licensed establishment for use of experimental animals (LUMC).

In Vivo SPECT Imaging and Quantitative Assessment Biodistribution

For biodistribution (n=4) and for single photon emission computed tomography (SPECT) imaging (n=2) approximately 40 MBq was injected intravenously. At 2 h post-injection, SPECT imaging was performed followed by *ex vivo* evaluation of the biodistribution (in total n=6 animals/tracer). Total-body imaging and data reconstruction of PC346C-tumour-bearing mice was performed on a U-SPECT scanner (MILabs, Utrecht, The Netherlands) according to previously described methods (*5,11*).

After imaging, animals were sacrificed by cervical dislocation and various tissues were resected, weighed and counted for radioactivity. Quantitative biodistribution measurements (percentage of the

injected dose per gram of tissue (% ID/g) and tumour-to-background ratios ($\frac{\%\frac{ID}{g}tumour}{\%\frac{ID}{g}background}$) were calculated.

Ex Vivo Fluorescence Imaging

Directly after SPECT imaging mice were sacrificed, fluorescence imaging was performed using a clinical grade laparoscope set-up (KARL STORZ Endoskope GMBh) (*15*). *Ex vivo* images of excised tissues were acquired at Cy5 (λ_{ex} = 640nm, λ_{em} = 680nm). For imaging with the fluorescence laparoscope, the tumour was placed on top of a height-adjustable lift and imaged with an identical setup as described previously (*11,15*). Images were acquired using a clinical grade IMAGE 1 S camera system equipped with a 0° laparoscope. Excitation was achieved using a Cy5-modified D-Light C light source (Cy5, KARL STORZ Endoskope GmbH & Co. KG, Tuttlingen, Germany). Detection of Cy5 was achieved by placement of an additional standard eyepiece adaptor (Cat. No. 20100034 KARL STORZ Endoskope GmbH & Co. KG) between the camera and the laparoscope (*11,15*).

Statistical Data Analysis

Analytical data were expressed as mean and standard deviation (± SD) as calculated using Graphpad Prism 7. The significance of two mean values was calculated using a Student's *t*-test or ANOVA. Outliers were detected and removed using the Grubb's method. The level of significance was set at $p \leq 0.05$.

Results

Chemistry

To allow identification of the most optimal interactions between the cyanine backbone and the amphipathic funnel, a series of five structurally related hybrid PSMA analogues was synthesised: EuK-Cy5-mas_3, EuK-(SO_3)Cy5-mas_3, EuK-Cy5(SO_3)-mas_3, EuK-(Ar)Cy5-mas_3, and EuK-Cy5(Ar)-mas_3 (Figure 1A and

1B). The 2-mercaptoacetyl-seryl-seryl-seryl chelate (mas_3; including a six-carbon spacer; Figure 1C) was conjugated to the respective indole of Cy5 dyes in 57–77% isolated yield. Consecutive addition of the tri-*tert*-butyl-protected ($EuK(tBu)_3$) targeting moiety to the orthogonal indole (35–89% isolated yield) followed by deprotection (18–98% isolated yield; Figure 1C) resulted in the final products. Comparing the yields of the four synthetic steps combined indicated that the introduction of a substituent on an indole and the position thereof influenced the synthetic ease: unsubstituted (32% yield) > benzene-containing (16–25% yield) > sulfonate-containing (3–6% yield).

Photophysical Properties

Compared to the unsubstituted EuK-Cy5-mas_3, the introduction of a sulfonate moiety on either indole (EuK-(SO_3)Cy5-mas_3, EuK-Cy5(SO_3)-mas_3) led to a slight increase in maximum excitation wavelength ($\lambda_{ex,max}$) and maximum emission wavelength ($\lambda_{em,max}$; bathochromic shift; Table 1). The introduction of an extra benzene moiety on either indole (EuK-(Ar)Cy5-mas_3, EuK-Cy5(Ar)-mas_3) increased this bathochromic shift to around 20 nm (Table 1, Supplemental Figure 2), which is in line with literature (*16*). However, the fluorescence brightness—the product of a fluorophore's molar extinction coefficient (ε; derived from the corresponding free fluorophore, Table SI1) and quantum yield (Φ_F)—of the tracer analogues with an extra benzene moiety on either indole was reduced by nearly 50%. This finding, which is in line with literature,(*15*) brings about a reduction in visibility compared to the sulfonate-containing tracers while using the same camera system and settings, thus making them less suitable for image-guided surgery. The brightness of EuK-(SO_3)Cy5-mas_3 was in the same range as the brightness described in previous literature on PSMA-targeting hybrid tracers ($0.8 \cdot 10^4$–$2.1 \cdot 10^4$ $M^{-1} \cdot cm^{-1}$) (*17-20*).

Absorption and emission spectra

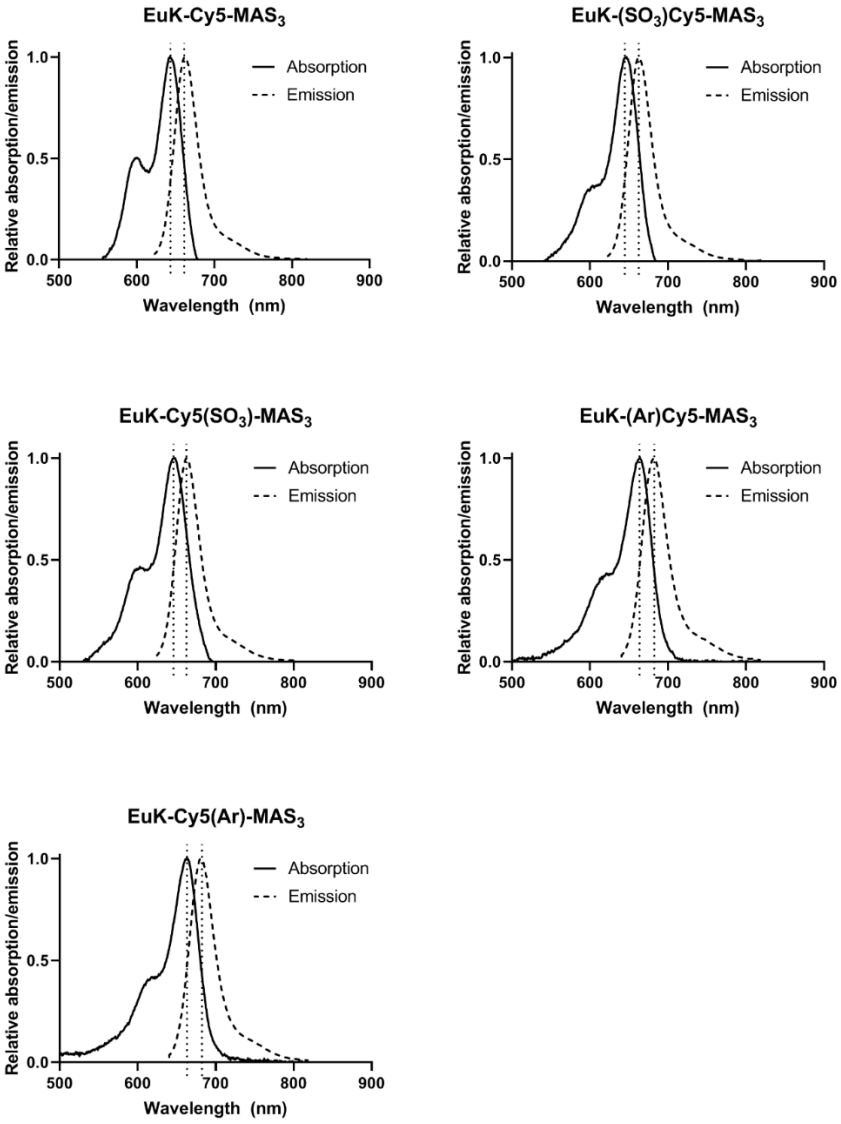

Supplemental Figure 10. Absorption (solid lines) and emission (dashed lines) spectra for all hybrid PSMA-targeting tracers. Dotted vertical lines represent the maximum absorption and emission wavelengths for each corresponding spectrum.

Compound	**Molar extinction coefficient in PBS (ε; $M^{-1} \cdot cm^{-1}$)**
Phth-Cy5-COOH	$9.30 \cdot 10^4$
Phth-(SO_3)Cy5-COOH	$1.46 \cdot 10^5$
Phth-Cy5(SO_3)-COOH	$9.50 \cdot 10^4$
Phth-(Ar)Cy5-COOH	$6.00 \cdot 10^4$
Phth-Cy5(Ar)-COOH	$3.70 \cdot 10^4$

Supplemental Table 1. Molar extinction coefficient of the free fluorophores $\varepsilon_{fluorophore}$ for the determination of the brightness of hybrid tracers.

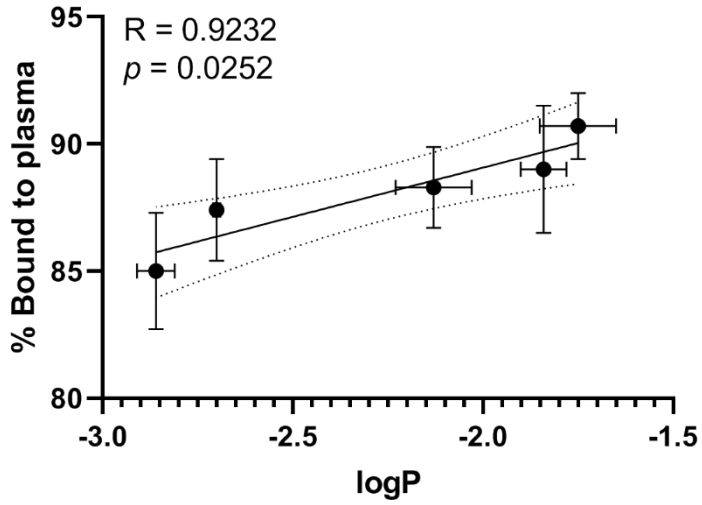

Supplemental Figure 11. Correlation between logP and PPB. Dotted lines represent 95% confidence interval

Compound	**Serum stability after 24 h (% remaining; ^{99m}Tc-mas$_3$ complex; n = 2)**
^{99m}Tc-EuK-Cy5-mas$_3$	88.5 ± 2.0%
^{99m}Tc-EuK-(SO$_3$)Cy5-mas$_3$	>99%
^{99m}Tc-EuK-Cy5(SO$_3$)-mas$_3$	>99%
^{99m}Tc-EuK-(Ar)Cy5-mas$_3$	>99%
^{99m}Tc-EuK-Cy5(Ar)-mas$_3$	>99%

Supplemental Table 2. ^{99m}Tc–mas$_3$ complex stability in serum after 24 h.

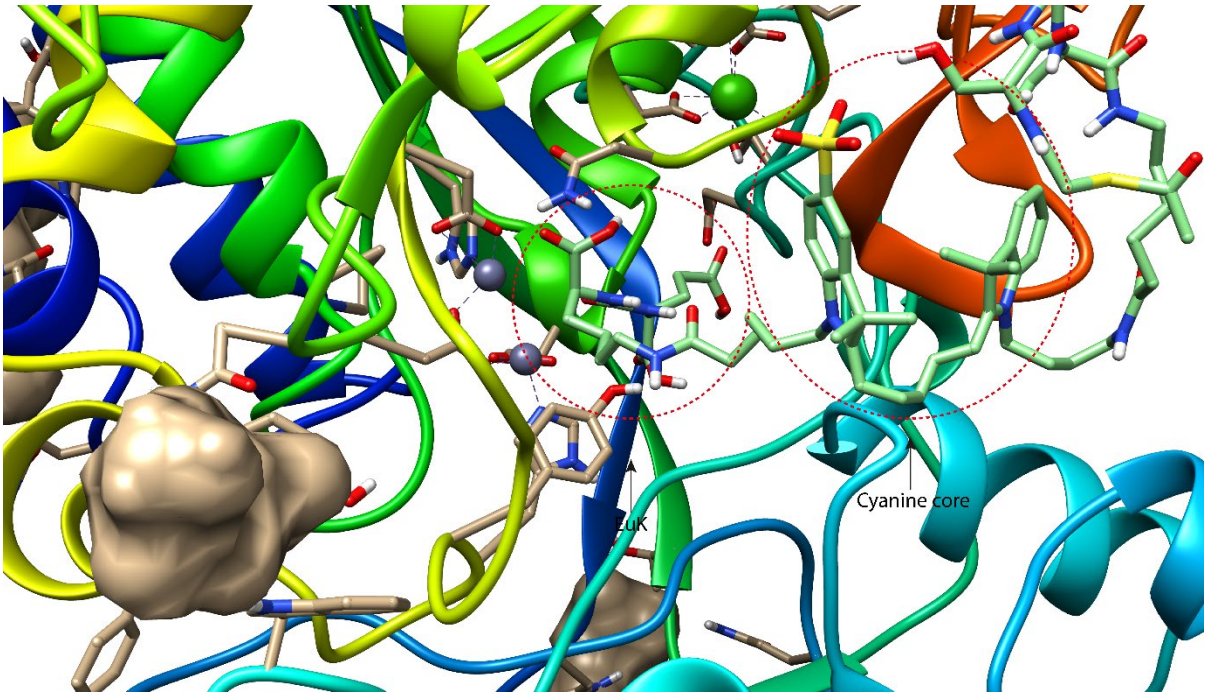

Supplemental Figure 12. Docking of EuK-(SO3)Cy5-mas3 in human glutamate carboxypeptidase II, or rather the prostate-specific membrane antigen (PSMA). PDB ID 2oot, docking with Autodock Vina, visualisation with UCSF Chimera. Binuclear zinc depicted as purple spheres.

Supplemental Table 3. *In vivo* biodistribution data at 2 h.

	^{99m}Tc-EuK-Cy5-mas$_3$	^{99m}Tc-EuK-(SO$_3$)Cy5-mas$_3$	^{99m}Tc-EuK-Cy5(SO$_3$)-mas$_3$	^{99m}Tc-EuK-(Ar)Cy5-mas$_3$	^{99m}Tc-EuK-Cy5(Ar)-mas$_3$
Blood	1.10 ± 0.15	0.24 ± 0.10	0.18 ± 0.07	2.32 ± 0.67	6.91 ± 1.08
Brain	0.02 ± 0.02	0.01 ± 0.01	0.01 ± 0.01	0.02 ± 0.02	0.03 ± 0.03
Lungs	1.77 ± 2.03	0.02 ± 0.01	0.02 ± 0.01	1.95 ± 1.35	0.82 ± 0.75
Heart	0.55 ± 0.08	0.17 ± 0.10	0.12 ± 0.06	1.07 ± 0.32	2.64 ± 0.80
Liver	1.82 ± 0.80	0.56 ± 0.45	0.45 ± 0.14	3.25 ± 2.18	9.64 ± 6.78
Kidneys	8.98 ± 5.78	18.35 ± 8.51	10.45 ± 12.83	15.64 ± 19.90	11.90 ± 12.26
Spleen	1.03 ± 0.72	0.97 ± 1.22	0.18 ± 0.19	0.39 ± 0.20	0.39 ± 0.20
Stomach	1.51 ± 1.19	1.74 ± 1.32	0.19 ± 0.11	0.82 ± 0.87	3.16 ± 2.11
Intestines	2.80 ± 2.35	1.61 ± 0.29	1.11 ± 0.68	6.62 ± 4.56	21.24 ± 13.40
Tumour	3.0 ± 2.4	15.27 ± 2.85	0.00 ± 0.00	3.47 ± 0.81	4.14 ± 3.33
Muscle	0.15 ± 0.16	0.17 ± 0.19	0.00 ± 0.00	0.37 ± 0.30	0.12 ± 0.16
Fat	0.05 ± 0.02	0.01 ± 0.00	0.00 ± 0.00	0.10 ± 0.08	0.20 ± 0.09
Salivary gland	0.08 ± 0.03	0.02 ± 0.01	0.02 ± 0.02	0.13 ± 0.07	0.23 ± 0.12
Prostate	0.71 ± 0.59	0.10 ± 0.06	0.03 ± 0.03	0.42 ± 0.40	1.37 ± 1.23
Tumour:blood	2.68 ± 2.16	70.15 ± 50.66	0.02 ± 0.02	0.65 ± 0.42	1.16 ± 0.01
Tumour:muscle	18.95 ± 14.66	5157.50 ± 949.17	0.46 ± 0.28	172.0 ± 84.95	5.79 ± 0.86
Tumour:prostate	4.22 ± 3.31	154.73 ± 28.48	0.02 + 0.00	10.36 ± 8.32	2.53 ± 0.59
Tumour:fat	60.07 ± 42.33	2578.75 + 474.59	0.65 ± 0.52	18.83 ± 1.30	46.50 ± 34.78
Tumour:kidney	2.75 ± 3.78	0.56 ± 0.14	0.00 ± 0.00	1.79 ± 2.40	1.61 ± 2.00

References

1. Pedersen DS, Rosenbohm C. Dry column vacuum chromatography. *Synthesis-Stuttgart.* 2001;2001:2431-2434.

2. Lopalco M, Koini EN, Cho JK, Bradley M. Catch and release microwave mediated synthesis of cyanine dyes. *Org Biomol Chem.* 2009;7:856-859.

3. Khan TH, Eno-Amooquaye EA, Searle F, Browne PJ, Osborn HM, Burke PJ. Novel inhibitors of carboxypeptidase G2 (CPG2): potential use in antibody-directed enzyme prodrug therapy. *J Med Chem.* 1999;42:951-956.

4. Makowski M, Rzeszotarska B, Smelka L, Kubica Z. Synthesis of Peptides with α,β-Dehydroamino Acids, III. Debenzyloxycarbonylation and Detrifluoroacetylation of Dehydroalanine and Dehydrophenylalanine Peptides. *Liebigs Annalen der Chemie.* 1985;1985:1457-1464.

5. Bunschoten A, van Willigen DM, Buckle T, et al. Tailoring Fluorescent Dyes To Optimize a Hybrid RGD-Tracer. *Bioconjug Chem.* 2016;27:1253-1258.

6. Mujumdar RB, Ernst LA, Mujumdar SR, Lewis CJ, Waggoner AS. Cyanine dye labeling reagents: sulfoindocyanine succinimidyl esters. *Bioconjug Chem.* 1993;4:105-111.

7. Hensbergen AW, van Willigen DM, Welling MM, et al. Click Chemistry in the Design and Production of Hybrid Tracers. *ACS Omega.* 2019;4:12438-12448.

8. Spa SJ, Hensbergen AW, van der Wal S, Kuil J, van Leeuwen FWB. The influence of systematic structure alterations on the photophysical properties and conjugation characteristics of asymmetric cyanine 5 dyes. *Dyes and Pigments.* 2018;152:19-28.

9. van der Wal S, Kuil J, Valentijn ARPM, van Leeuwen FWB. Synthesis and systematic evaluation of symmetric sulfonated centrally C C bonded cyanine near-infrared dyes for protein labelling. *Dyes and Pigments.* 2016;132:7-19.

10. Weineisen M, Simecek J, Schottelius M, Schwaiger M, Wester HJ. Synthesis and preclinical evaluation of DOTAGA-conjugated PSMA ligands for functional imaging and endoradiotherapy of prostate cancer. *EJNMMI Res.* 2014;4:63.

11. Buckle T, van Willigen DM, Spa SJ, et al. Tracers for Fluorescence-Guided Surgery: How Elongation of the Polymethine Chain in Cyanine Dyes Alters the Pharmacokinetics of a Dual-Modality c[RGDyK] Tracer. *J Nucl Med.* 2018;59:986-992.

12. Trott O, Olson AJ. AutoDock Vina: improving the speed and accuracy of docking with a new scoring function, efficient optimization, and multithreading. *J Comput Chem.* 2010;31:455-461.

13. Pettersen EF, Goddard TD, Huang CC, et al. UCSF Chimera--a visualization system for exploratory research and analysis. *J Comput Chem.* 2004;25:1605-1612.

14. Marques RB, van Weerden WM, Erkens-Schulze S, et al. The human PC346 xenograft and cell line panel: a model system for prostate cancer progression. *Eur Urol.* 2006;49:245-257.

15. van Willigen DM, van den Berg NS, Buckle T, et al. Multispectral fluorescence guided surgery; a feasibility study in a phantom using a clinical-grade laparoscopic camera system. *Am J Nucl Med Mol Imaging.* 2017;7:138-147.

16. Sauer M, Hofkens J, Enderlein J. Basic Principles of Fluorescence Spectroscopy. In: Sauer M, Hofkens J, Enderlein J, eds. *Handbook of Fluorescence Spectroscopy and Imaging*. Weinheim, Germany: Wiley; 2011:1-30.

17. Banerjee SR, Pullambhatla M, Byun Y, et al. Sequential SPECT and optical imaging of experimental models of prostate cancer with a dual modality inhibitor of the prostate-specific membrane antigen. *Angew Chem Int Ed Engl.* 2011;50:9167-9170.

18. Baranski AC, Schafer M, Bauder-Wust U, et al. Improving the Imaging Contrast of (68)Ga-PSMA-11 by Targeted Linker Design: Charged Spacer Moieties Enhance the Pharmacokinetic Properties. *Bioconjug Chem.* 2017;28:2485-2492.

19. Kommidi H, Guo H, Nurili F, et al. (18)F-Positron Emitting/Trimethine Cyanine-Fluorescent Contrast for Image-Guided Prostate Cancer Management. *J Med Chem.* 2018;61:4256-4262.

20. Schottelius M, Wurzer A, Wissmiller K, et al. Synthesis and Preclinical Characterization of the PSMA-Targeted Hybrid Tracer PSMA-I&F for Nuclear and Fluorescence Imaging of Prostate Cancer. *J Nucl Med.* 2019;60:71-78.